Atmos. Chem. Phys. Discuss., 14, 27373–27424, 2014
www.atmos-chem-phys-discuss.net/14/27373/2014/
doi:10.5194/acpd-14-27373-2014

Atmospheric Chemistry and Physics Discussions

Direct measurements of near-highway emissions in a high diesel environment

H. L. DeWitt[1], S. Hellebust[1], B. Temime-Roussel[1], S. Ravier[1], L. Polo[2,3], V. Jacob[2], C. Buisson[3], A. Charron[3], M. André[3], A. Pasquier[3], J. L. Besombes[4], J. L. Jaffrezo[2], H. Wortham[1], and N. Marchand[1]

[1]Aix Marseille Université, CNRS, LCE FRE 3416, 13331 Marseille, France
[2]Université Grenoble Alpes, CNRS, LGGE, 38000 Grenoble, France
[3]IFSTTAR, Case 24, 69675 Bron Cédex, France
[4]Université de Savoie, LCME, 73376 Le Bourget-du-Lac, France

Received: 26 September 2014 – Accepted: 2 October 2014 – Published: 30 October 2014

Correspondence to: H. L. DeWitt (helen-langley.dewitt@univ-amu.fr) and N. Marchand (nicolas.marchand@univ-amu.fr)

Published by Copernicus Publications on behalf of the European Geosciences Union.

Abstract

Diesel-powered passenger cars currently outnumber gasoline-powered cars in many countries, particularly in Europe. In France, diesel cars represented 61 % of Light Duty Vehicles in 2011 and this percentage is still increasing (French Environment and Energy Management Agency, ADEME). As part of the September 2011 joint PM-DRIVE (Particulate Matter- DiRect and Indirect on-road Vehicular Emissions) and MOCOPO (Measuring and mOdeling traffic COngestion and POllution) field campaign, the concentration and high-resolution chemical composition of aerosols and volatile organic carbon (VOC) species were measured adjacent to a major urban highway south of Grenoble, France. Alongside these atmospheric measurements, detailed traffic data were collected from nearby traffic cameras and loop detectors, which allowed the identification of vehicle type and characteristics, traffic concentration, and traffic speed to be quantified and compared to measured aerosol and VOCs. Six aerosol age and source profiles were resolved using the positive matrix factorization (PMF) model on real-time high-resolution aerosol mass spectra. These six aerosol source/age categories included a hydrocarbon-like organic aerosol (HOA) commonly associated with primary vehicular emissions, a nitrogen containing aerosol (NOA) with a diurnal pattern similar to that of HOA, oxidized organic aerosol (OOA), and biomass burning aerosol (BBOA). While quantitatively separating the influence of diesel vs. gasoline proved impossible, a low HOA : black carbon ratio, similar to that measured in other high-diesel environments, and high levels of NO_x, also indicative of diesel emissions, were observed. A comparison between these high-diesel environment measurements and measurements taken in low-diesel (North American) environments was examined and the potential feedback between vehicular emissions and SOA formation was probed. Although the measurement site was located next to a large source of primary emissions, which are typically found to have low oxygen incorporation, OOA was found to comprise the majority of the measured organic aerosol, and the measured OOA contained mainly modern carbon, not fossil-derived carbon. Thus, even in this heavily

ACPD
14, 27373–27424, 2014

vehicular-emission impacted environment, photochemical processes, biogenic emissions, and aerosol oxidation dominated the overall organic aerosol mass measured during most of the campaign.

1 Introduction

Aerosols are known to have adverse effects on human health and the global climate. The World Health Organization (WHO) recently added anthropogenic aerosol and air pollution to their list of known carcinogens (WHO, 2013), and high mass concentrations of particles less than 2.5 micrometers in diameter ($PM_{2.5}$), such as those emitted by vehicular combustion processes, are particularly harmful (Lighty et al., 2000). Vehicular traffic is a large source of submicrometer anthropogenic aerosol and proximity to large sources of vehicular emissions has been shown to increase lung and heart disease, especially in children (Brugge et al., 2007). For vehicular aerosol emissions, factors such as the fuel used (diesel vs. gasoline), age of the car engine, and highway speed (stop and go traffic vs. constant speed) can affect the concentration and physical and chemical composition of the aerosol emitted. A recent WHO report examined the toxilogical effects of black carbon (BC) aerosol, a known emission of diesel vehicles. Although no difference in toxicology between $PM_{2.5}$ and BC aerosol inhalation was found, BC was cited as a marker for more general vehicular emissions, which have been shown to have negative health effects; diesel exhaust was added as a known carcinogen the year before general air pollution and $PM_{2.5}$ (Janssen, World Health Organization, 2012). Aside from the potential detrimental health effects of BC, BC also has significant implications for climate change. Unlike the majority of aerosol (e.g., most organic aerosol, ammonium sulfate, ammonium nitrate), BC aerosol is associated with global warming due to its high absorption of solar radiation (Bond et al., 2013). Diesel vehicles have been singled out as important sources of BC to regulate as, unlike most other BC sources, diesel vehicles tend not to co-elute high concentrations of other, less

ACPD
14, 27373–27424, 2014

absorbing (thus more cooling) aerosol and therefore have a higher net heating effect than mixed-emission black carbon sources (Bond et al., 2013).

In France, the lower cost of diesel fuel (due to a lower taxation rate of diesel fuel vs. gasoline fuel) and the generally higher fuel efficiency of diesel engines have caused diesel passenger cars to outnumber gasoline passenger cars: in 2011 diesel cars represented 60 % of the total vehicular fleet (Light Duty Vehicles, LDV) (61 % in 2013) according to the French Environment and Energy Management Agency (ADEME). The influence of diesel vehicles increases if we consider the total fuel consumption per capita, which better captures the use of diesel and gasoline vehicles on the road (road sector only, World Bank, 2011). In 2011, 82 % of the fuel consumed in France was diesel (World Bank, 2011). For comparison, this percentage in 2011 was 28 % in the US, 57 % in China, 70 % in the European Union, 49 % in Latin America and the Middle East, and 83 % in low-income countries.

The emission characteristics and emission limits of these two types of engines (diesel and gasoline) are quite different: diesel vehicles have higher emission rates for primary organic aerosol (POA) and BC, while gasoline-powered vehicles have higher emission rates for carbon monoxide (CO), carbon dioxide (CO_2), and volatile organic carbon (VOCs) (e.g., toluene, benzene) (Platt et al., 2013). Black carbon, in particular, is closely associated with diesel: in Europe, North America, and Latin America, an estimated 70 % of BC emissions are from diesel-powered vehicles (Bond et al., 2013). These differences in emissions were observed in studies performed in Mexico City, where particulate and VOC emissions were measured both at stationary measurement sites and during vehicular chases with the Aerodyne Mobile Laboratory (Thornhill et al., 2010). During this study, diesel and gasoline vehicles on the road were manually counted and specific vehicles were followed and their emissions captured. From these data, diesel was found to contribute almost all of the BC mass and particle number concentration, along with the majority of $PM_{2.5}$, while gasoline emissions were found to have elevated levels of toluene and benzene (Thornhill et al., 2010). In Marseille, France, a traffic tunnel experiment measured an organic carbon/elemental carbon ra-

ACPD
14, 27373–27424, 2014

tio (OC/EC) in $PM_{2.5}$ of 0.3–0.4, which indicates that significant amounts of black carbon is emitted from local traffic in Marseille (El Haddad et al., 2009). Recent measures have been taken in Europe to reduce the particulate emission from diesel vehicles: from Euro 4 to Euro 5, a diesel particle filter (DPF) was introduced in diesel vehicles and the regulated emission limit for $PM_{2.5}$ was halved for diesel cars and trucks.

Outside of smog-chamber studies, both aerosol and VOC emissions from both vehicle types, as well as biogenic emissions, industrial emissions, and emissions from other sources, will react together in the atmosphere and potentially form secondary organic aerosol (SOA). Thus, primary aerosol emissions may not be the most important emission factor to take into account for global reduction in anthropogenic aerosol. After emission, VOCs can react in the atmosphere and form SOA. From these reactions, gasoline VOC emissions could ultimately lead to the formation of higher concentrations of organic aerosol than organic aerosol released directly from diesel vehicles, as reported in a recent study comparing the SOA formation from a Euro 3 diesel LDV and a Euro 5 gasoline LDV (Platt et al., 2013).

Smog chamber measurements and field studies on vehicular emissions are important as differences in the SOA formation potential of diesel and gasoline gas- and particle-phase emissions are not fully understood. A recent study by Bahreini et al. (2012) measured similar levels of SOA in the heavily traffic-influenced LA Basin during both weekend and weekday afternoons. While diesel-powered vehicle numbers on the road decrease significantly on the weekends in the LA area, the measured SOA does not, which leads to the conclusion that gasoline emissions are more responsible for SOA than diesel emissions (Bahreini et al., 2012). Nordin et al. (2013) performed smog-chamber studies on SOA formation from gasoline-vehicle VOC emissions during simulated cold start and idling driving conditions, and confirmed the high potential of SOA formation from gasoline car exhaust. They show that after a cumulative OH exposure of $\sim 5 \times 10^6$ cm^{-3} h^{-1}, the formed SOA was 1–2 orders of magnitude higher than the primary OA emissions. Another recent paper calculates the reactivity potential of diesel and gasoline fuel and comes to the opposite conclusion: that due to the reactivity

ACPD
14, 27373–27424, 2014

potential of diesel fuel, diesel-powered vehicles should contribute greater amounts of SOA than gasoline-powered vehicles to the atmosphere (Gentner et al., 2012).

Finally, gas-phase NO and NO_2 (NO_x) ambient concentrations are also associated with diesel fuel use (Vestreng et al., 2009). Throughout Europe, while NO_x emission standards for diesel vehicles have increased in stringency in recent years, ambient NO_2 levels have not shown a corresponding decrease (Vestreng et al., 2009). The reduction of atmospheric NO_x is important for health-related reasons as an increase in NO_x leads to an increase in tropospheric ozone, which is a known lung irritant. NO_x levels have also been shown to affect the formation rate, formation pathways, and chemical composition of secondary organic aerosol from the reaction of primary species in numerous chamber studies (Carlton et al., 2009; Kroll et al., 2005; Ng et al., 2007, 2008; Presto et al., 2010).

European vehicular emissions, near-highway pollution levels, and the chemical composition of highway pollution may be quite different than those measured in North America due to many factors, including: (1) different emission standards and fuel regulations, (2) different after-treatment devices to reduce the emission of certain pollutants and (3) a much larger percentage of diesel-powered passenger cars on the road. A comparison between European and North American near-highway measurements could lead to further understanding of the effects of diesel vs. gasoline on near-highway atmospheric chemistry.

To fully categorize the aerosol, VOC, and NO_x emissions of traffic in France, the joint PM-DRIVE (Particulate Matter-DiRect and Indirect on-road Vehicular Emissions) and MOCOPO (Measuring and mOdeling traffic COngestion and POllution) field mission took place in the Grenoble basin, France during the fall of 2011 at a near-highway location south of the city center. These measurements were part of a larger campaign that including direct tail-pipe emission measurements and smog chamber studies. During the field measurements discussed in this paper, traffic cameras allowed the vehicle type determination through license plate automatic identification and traffic densities, speed and total flow were quantified through loop detectors, while measurements of

ACPD
14, 27373–27424, 2014

the chemical composition, concentration, and size of aerosol were collected using both real-time and offline analysis, and parallel data on the gas-phase chemical composition of the roadway-adjacent environment were also collected. A source apportionment model was applied to real-time aerosol chemical composition data. Particular attention was paid to the chemical composition of particles and VOCs emitted during morning and evening rush hours in an attempt to elucidate the primary vehicular influence on near-highway air pollution.

2 Experimental methods

2.1 Description of the measurement site

The sampling site was located at 45.150641° N, 5.726028° E (Fig. 1), just south of Grenoble, France adjacent to a major highway (south of E712, with A480 2 km to the East). During the week, the total traffic on the highway was about 95 000 vehicles day^{-1} (65 000 during the weekend). Grenoble, a large city with over half a million people, is located in the southeast of France at the foothills of the Alps. The surrounding mountain ranges both buffer the Grenoble area from the effects of transported aerosol and can also trap pollution within the valley, particularly during the winter months and periods of temperature inversions. The isolating effect of the mountains thus simplifies the potential sources for aerosol, making it an interesting location for the study of specific aerosol emission sources.

2.2 Traffic cameras and loop detectors

Traffic cameras mounted to a roadway sign were used to capture the license plate numbers of vehicles driven on the highway close to the field measurement site. These numbers were later used to classify vehicular traffic into different categories: vehicle type (LDV, Heavy duty vehicles (HDV), buses) and age, vehicle size and engine capacity, fuel type (diesel or gasoline), and Euro number (i.e. the pollutant emission regulation

ACPD
14, 27373–27424, 2014

that the vehicle complies with), The speed of the passing vehicles was also monitored with the classical traffic detector (double electromagnetic loops, able to identify the passing of all vehicles and their speeds), which allowed the identification of periods of stop-and-go, dense, or free-flow traffic.

2.3 Massalya platform

The MASSALYA platform is a mobile laboratory equipped for air quality measurements with a hub located at the Aix Marseille Université. For the field campaign, $PM_{2.5}$ and PM_1 sampling heads situated above the roof of the stationary truck were connected to a variety of online instrumentation located within the truck body. Complementary off-line analysis was performed on filter samples collected by HiVol samplers located adjacent to the MASSALYA platform. All sampling occurred approximately 15 m from one of the traffic lines. Further details can be found in Polo-Rehn (2013).

A High-Resolution Time-of-Flight Aerosol Mass Spectrometer (Aerodyne, HR-ToF-AMS) was used to analyze the chemical composition, size, and concentration of non-refractory submicrometer particles in the ambient atmosphere (DeCarlo et al., 2006). Instrument specifications have been discussed in detail elsewhere (DeCarlo et al., 2006). Briefly, both high resolution and size-speciated chemical information for ambient aerosol were obtained from this instrument. Aerosols were vaporized at 600 °C, ionized using electron ionization (EI) at an energy of 70 eV, and the chemical composition of bulk aerosol was measured using a ToF mass spectrometer (TOFWERK). Aerosol spectra were continuously collected and a two minute average spectrum was obtained. Aerosol vacuum aerodynamic diameter was calculated by setting a particle start time using a chopper wheel and measuring the particle flight time along the particle ToF (pToF) sizing region (DeCarlo et al., 2006). Typical resolution during the campaign was around $2800 m/\Delta m$ (where $m = m/z$ and Δm = full-width at half max of the mass peak).

In addition to the HR-ToF-AMS, a Size-Mobility Particle Scanner (TSI, SMPS) was used to measure the size distribution and concentration of ambient aerosol and a Mul-

ACPD
14, 27373–27424, 2014

tiangle Absorption Photometer (Thermofischer, MAAP 5012) was used to measure the concentration of black carbon.

High resolution mass spectra of VOCs were obtained using an Ionicon Proton-Transfer Reaction Time of Flight Mass Spectrometer 8000 (PTR-ToF-MS, hereafter referred to as PTR-MS) (Graus et al., 2010). The PTR-MS analyzes trace (parts per trillion by volume) VOCs with high mass resolution, which allows the separation of different species with the same nominal mass and the identification of each peak's elemental formula. The PTR-MS was run with a 25 s time resolution and a flow of 100 $cm^3\,min^{-1}$. Drift tube parameters of the PTR-MS were as follows: voltage: 560 V, drift tube pressure: 2.11 mbar, drift tube temperature: 333 K, resulting in an E/N (electric field/number concentration of neutral particles) of 133 Td.

The SMPS, PTR-ToF-MS, and HR-ToF-AMS were connected to the same sample inlet with a $PM_{2.5}$ sampling head and a sample flow of 1 $m^3\,h^{-1}$. Particles were dried (RH < 30 %) using a Nafion dryer prior to measurement with the HR-ToF-AMS and SMPS. The MAAP was connected to a separate PM_1 sampling head. PM_1 filter HiVol (30 $m^3\,h^{-1}$) samples were collected on quartz filters (Tissuquartz) on a daily basis and analyzed for radiocarbon isotope data. Radiocarbon measurements were conducted using ARTEMIS Accelerator Mass Spectrometry, at Saclay (CNRS-CEA-IRD-IRSN, France) on the total carbon (TC) fraction. The method is fully described in El Haddad et al. (2011).

A Young meteorological station was also installed to capture wind speed, wind direction, relative humidity, and temperature data at the measurement location.

2.4 Air Rhône Alpes station

Twenty meter to the East along the highway, the Air Rhône Alps station collected $PM_{2.5}$ HiVol (30 $m^3\,h^{-1}$) samples on quartz fiber filters (Tissuquartz) with a time resolution of 4 h. $PM_{2.5}$ samples were analyzed for EC/OC, inorganic ions, and targeted organic tracers (Polo-Rehn, 2013).

ACPD
14, 27373–27424, 2014

Organic compounds in these PM samples were also quantified by gas chromatography coupled with mass spectrometry (GC-MS), following the method detailed in El Haddad et al. (2009) and Favez et al. (2010). EC and OC measurements were performed using the Thermo-Optical Transmission (TOT) method on a Sunset Lab analyzer (Birch and Cary, 1996; Jaffrezo et al., 2005) following the EUSAAR2 temperature program (Cavalli et al., 2010). Ionic species were analyzed with Ionic Chromatography (IC) following the method described in Jaffrezo et al. (1998).

All filters used in this study were preheated at 500 °C during 3 h. Samples were stored at −18 °C in aluminum foil and sealed in polyethylene bags until analysis.

In addition, NO_x (NO and NO_2), PM_{10} and $PM_{2.5}$ mass concentrations were measured and a Tapered Element Oscillating Microbalance equipped with a Filter Dynamic Measurement System (TEOM-FDMS, Thermo Scientific) for real-time measurements of PM_{10} and $PM_{2.5}$.

3 Results and discussion

3.1 Traffic conditions at the measurement site

The correlation of diesel and gasoline vehicles (data averaged for 15 min) and four hour averages of the vehicle type (LDV, HDV, and buses) and Euro number of passing vehicles are shown in Fig. 2a and b, respectively. The overall makeup of the traffic remained fairly steady throughout the campaign. LDVs accounted for the majority of traffic (94 %) and only experienced a small drop-off in flow over the weekends (87 % of the weekday flow). HDVs and buses, however, were present in much higher concentrations during the week vs. the weekend (2.7 times less buses and HDVs on the weekends), and also were in lower numbers on the road during the early morning and late evening hours. The ratio of LDVs to HDVs increased by a factor of 4 from the morning rush hour peak to the evening rush hour peak.

ACPD
14, 27373–27424, 2014

The bulk of the vehicles directly affecting the measurement site were Euro 4 (released in 2005) or older; thus, the most recent emission regulations had only a small effect on the air quality around the field site. From the 15 min time-resolution traffic data (not shown), approximately five times as many Euro 4 as Euro 5 cars were counted on the road during the measurement period, while similar numbers of Euro 3 and Euro 4 cars were observed. A relatively high correlation between the different Euro classifications of vehicles was observed (R^2 values of 0.7 for Euro 5 and Euro 4, 0.9 for Euro 3 and Euro 4, using 15 min time resolution traffic data). For diesel cars, from Euro 4 (released in 2005) to Euro 5 (released in 2009), NO_x emission limits decreased from 0.25 to 0.18 g km^{-1} and particulate emission limits decreased from 0.025 to 0.005 g km^{-1}. From Euro 3 (released in 2000) to Euro 4 another two-fold decrease in NO_x and PM emission limits was implemented for diesel vehicles. Gasoline NO_x emission limits were reduced from 0.15 to 0.08 to 0.06 g km^{-1} from Euro 3 to Euro 5, and total hydrocarbon emission limits were reduced from 0.20 to 0.10 g km^{-1} from Euro 3 to Euro 4. No PM limits were implemented for gasoline-powered vehicles until Euro 5, where a limit of 0.005 g km^{-1} for direct-injection vehicles was introduced, and no total hydrocarbon emission limits have been introduced for diesel-powered vehicles.

As both diesel and gasoline engines are used to power passenger cars in France, a high correlation ($R^2 = 0.96$) between diesel and gasoline vehicles on the highway was found (Fig. 2b). The ratio between diesel and gasoline (the slope of the line) was found to be 2.6, or 72 % diesel. This value is slightly higher than that reported by ADEME for French vehicle fleet (61 %). However, ADEME data represent the registered vehicles and not the on-road vehicles. This difference highlights the combined effects of fuel costs and of vehicles consumption. Additionally, no weekly variation (weekend vs. weekday) in the ratio of diesel: gasoline powered vehicles on the road was observed, unlike that commonly observed on North American highways (Bahreini et al., 2012).

ACPD
14, 27373–27424, 2014

3.2 General atmospheric conditions and aerosol and VOC concentrations and evolution

Wind speeds were generally low throughout the campaign (< 1–$2\,m\,s^{-1}$) with higher wind speeds peaking in the afternoons and tapering off in the evenings. The wind direction was primarily from the northwest implying that the measurements station usually downwind from the highway.

The campaign time series concentration of submicrometer non-refractory aerosol sulfate (SO_4), ammonium (NH_4), nitrate (NO_3), and organic species from the HR-ToF-AMS is shown in Fig. 3a. The limit of detection for each species was calculated using the method described by DeCarlo et al. (2006) and found to be 0.30, 0.21, 0.06, and $0.33\,\mu g\,m^{-3}$ for SO_4, NH_4, NO_3, and organic aerosol, respectively, for our measurements with a time resolution of 2.5 min. A collection efficiency (CE) of 0.75 was applied to HR-ToF-AMS aerosol concentration measurements taken during this campaign. The CE factor compensates for incomplete vaporization of non-refractory species due to particle bounce, the likelihood of which changes with particle phase and chemical speciation (Huffman et al., 2005; Matthew et al., 2008). This CE was calculated by comparing the HR-ToF-AMS SO_4 concentrations to 4 h filter concentrations (S1). This comparison gave a value of 0.75 ± 0.03 for the slope between the two types of measurements.

$PM_{2.5}$ averaged $17\,\mu g\,m^{-3}$ for the campaign (Fig. S2) while PM_{10} averaged $22\,\mu g\,m^{-3}$. Black carbon and organic aerosol species dominated the measured aerosol composition throughout the campaign (Fig. 3a), and comprised 39 and 40 % of the total speciated submicrometer aerosol, respectively. Increases in BC and the aerosol marker m/z 57 ($C_4H_9^+$), a marker for primary organic carbon in the HR-ToF-AMS (Zhang et al., 2005), correlated in time to the observed morning and evening traffic peaks (Fig. 3b), with BC levels reaching 10–16 $\mu g\,m^{-3}$ during the mornings (Fig. 3a) for 2.5 min averaged measurements. Note that BC concentrations during high filter loadings (BC accumulation rate $> 0.14\,\mu g\,min^{-1}$) have been removed to compensate for the under-

ACPD
14, 27373–27424, 2014

estimation of BC by the MAAP during periods of high concentrations (Hyvärinen et al., 2013). Along with increased concentrations of m/z 57 and BC, elevated number concentrations of small particles (up to 1–2 × 10^5 cm^{-3} during peaks from daily base levels of 2–4 × 10^4 cm^{-3}) were observed during periods of heavy traffic (Fig. 3d), for 5 min measurements. BC and m/z 57 had similar daily averages throughout the campaign; however, overall organic concentration rose significantly during the period from 12–14 September, when particle growth events were observed (Fig. 3d). The geometric number mode diameter rose over the course of each day to a maximum diameter each afternoon, when photochemical processing was the most intense. A marker for oxidized, aged organic aerosol (Fig. 3c, m/z 44, COO^+) also rose in concentration during this time period, further confirming that the larger aerosol and higher organic mass concentrations were due to aging and secondary organic aerosol formation processes. A period of heavy rain on the 18th and 19th of September removed much of the organic aerosol from the local atmosphere. Black carbon concentrations and small particle concentrations quickly returned to their previous levels. A new accumulation period was observed after rainfall (Fig. 3d), with the mode diameter of particles increasing as secondary aerosol was formed again.

These findings are similar to those presented recently by Sun et al., (2012), who measured aerosol size and chemical composition adjacent to the Long Island Expressway in New York and observed that traffic-influenced aerosol emissions were primarily small particles which varied in concentration with changes in traffic throughout the day. During periods with less traffic influence, more oxygenated organic aerosol (OOA) and inorganic ions with larger mode diameters and lower temporal variations were observed (Sun et al., 2012).

The time series concentrations of selected VOC peaks are shown in Fig. 4. Primary traffic related VOC species, such as aromatics (benzene and toluene), were found to have high temporal variations similar to those of traffic-related aerosol species and NO_x (Fig. 4c and d). NO_x levels were often over 400 ppbv during the morning rush hours, while the PTRMS peak corresponding (in part) to toluene and benzene peaked

ACPD
14, 27373–27424, 2014

around 2 to 1 ppbv (respectively). During a recent chamber study in Ispra, Italy, the PTR-MS VOC spectra from fresh diesel emissions were found to contain peaks with the same mass as $CH_4NO_2^+$ and $C_2H_5O^+$ (Hellebust et al., 2013, 2014), not present in fresh gasoline emissions. These same peaks were also observed during this work and found to vary with traffic during this measurement period, but had a smoother variation than the observed aromatics (Fig. 4b). While this species is unique for fresh diesel emissions vs. gasoline emissions, aging processes occur rapidly and other sources may contribute to this mass peak. Thus, these species, while increasing with traffic, cannot be assumed to be tracers for primary diesel emissions in particular; no high-concentration unique tracer peak for diesel VOC emissions was resolved from the fresh diesel emission spectra in these chamber experiments (Hellebust et al., 2014).

In addition to traffic-related VOC emissions, mass peaks corresponding in exact mass to biogenic emissions, such as isoprene, were measured in ppbv levels. These peaks were found to rise in concentration with the ambient temperature (Fig. 4a), typical of isoprene peaks. The presence of isoprene and its oxidation product, methyl vinyl ketone (MVK) or its isomer methacrolein (MACR), in similar concentrations as that of the major traffic-related VOC peaks (ppbv levels) suggested that biogenic emissions also significantly influenced the local atmosphere despite close proximity to anthropogenic emission sources (i.e., road traffic).

The high morning concentrations of traffic-related pollutants, compared to evening concentrations, were caused in part by a low early morning boundary layer that rose during the day and fell during the night. Boundary layer heights (BLH) were estimated using the Hybrid Single Particle Lagrangian Integrated Trajectory (HYSPLIT) backtrajectory model. The HYSPLIT model either extracts the BLH from meteorological file input into the model or, if no BLH exists in the meteorological file, BLH is estimated using the vertical temperature profile. A selection of the BLH corrected diurnal profiles of traffic and biogenic emission related VOC concentrations are shown in Fig. 5a along with traffic (speed, vehicular flux) diurnal profiles and the calculated boundary layer heights and measured temperatures (Fig. 5b and c). Biogenic species, such as

ACPD
14, 27373–27424, 2014

isoprene, peaked in concentration during the afternoon, when temperatures were the warmest. Aromatic species peaked in concentration, even after the rough boundary layer correction was applied, during periods of low speeds. This is consistent with other findings that show cold starts and idling speeds cause an increase in aromatic VOC emissions from gasoline-powered vehicles (e.g., Broderick and Marnane, 2002)

Figure 6 shows the correlation between diurnally-averaged BC concentrations and vehicle flux. The markers are colored by the diesel : gasoline ratio and the marker size corresponds to the vehicle speed. The diesel : gasoline ratio varied from 2.4–3.6 and had little observable effect on the BC : vehicle number ratio. Vehicle flux and BC negatively correlated with vehicle speed, indicating that both the number of vehicles and traffic flow (stop-and-go vs. steady flow) likely influenced vehicular emissions.

3.3 Aerosol size-resolved chemical composition

Both pToF AMS and SMPS data show that the prominent particle mode was significantly smaller during periods of heavy traffic than during periods of low traffic influence. In the afternoon, and particularly during periods with increased concentration of SOA, the SMPS number-weighted geometric mode diameter rose (Fig. 3d). To study the chemical differences between particles of different sizes, the size-resolved aerosol mass spectra was probed. The calculation of the HR-ToF-AMS spectra for five different size bins revealed that organic aerosol dominated the lowest (50–90 nm) size range while sulfate and nitrate contributed more significantly to the larger (greater than 165 nm) aerosol particles (Fig. 7). The size-resolved concentrations of m/z 57 ($C_4H_9^+$) and 44 (COO^+) were also examined and found to have opposite correlations with size: the POA hydrocarbon tracer peak (m/z 57) dominated the aerosol spectra in the small sizes, while the aged, oxidized organic aerosol tracer peak (m/z 44) dominated the larger sizes (Fig. 7, Fig. S3).

Thus, traffic emissions greatly influenced the number concentration of aerosol, and most of the traffic aerosol was comprised of hydrocarbons. However, oxidized organic species and inorganic species dominated the overall mass concentration of aerosol

ACPD
14, 27373–27424, 2014

due to their larger size. Both the HR-ToF-AMS and SMPS size distributions during high- and low-traffic periods measured in this field campaign agreed with previous findings that direct traffic particulate emissions are primarily comprised of small particles (e.g., Sun et al., 2012).

3.4 PMF analysis

The positive matrix factorization (PMF) model was applied to the HR-ToF-AMS aerosol data using the process described in detail by Ulbrich et al. (2009). Six aerosol factors were resolved by their source and relative aging using the PMF model: a hydrocarbon-like organic aerosol (HOA) factor, a regional oxidized organic aerosol (OOA) factor associated with sulfate aerosol, two oxidized organic aerosol factors with opposing diurnal patterns, one more oxidized than the other (Less Oxidized Organic Aerosol, or LO-OA, with peak concentration during the mornings/nights, and More Oxidized Organic Aerosol, or MO-OA, with peak concentrations during the afternoons), a biomass-burning organic aerosol factor (BBOA), and a nitrogen-containing organic aerosol factor (NOA) (Figs. 8–10). The mass spectra for the six resolved factors in Fig. 8, labeled with their identifications. Evaluation graphs for the six-factor PMF solution are shown in the Supplement (Figs. S4–S6). Polar plots of the factor concentrations and wind direction are shown in Fig. S8. A six factor solution was the lowest number of factors where a BBOA factor was resolved; BBOA was suspected to be present in the air mass measured during the campaign due to periods of increased levoglucosan measured on filter samples. However, its concentrations were very low (15 ng m^{-3} on average, Polo-Rehn, 2013) compared to concentrations measured in Grenoble in winter (around 800 ng m^{-3}, Herich et al., 2014). Solutions with more than six factors appeared to split the OOA factor further until differences between each OOA factor were difficult to justify.

The diurnal pattern and the relative concentrations of each resolved factor, averaged over the campaign period, are shown in Fig. 9, along with the SD of their concentrations. Morning and evening peaks, correlating in time to rush hour traffic, were clearly observable for the HOA factor. Also clearly visible in Fig. 9a is the opposing diurnal

ACPD
14, 27373–27424, 2014

trends of LO-OA (peaking at night and early morning) and MO-OA (peaking around 3 p.m. each afternoon). Regional OOA had no discernable diurnal trend. An interesting finding in these data is that the HOA and NOA factor concentrations both peaked during morning and evening high traffic periods (Fig. 9a). This is not the general behavior demonstrated in most studies for the NOA factor, although a similar NOA factor has been previously measured in the Po Valley, Italy (Saarikoski et al., 2012). While many of the defined N-containing peaks were adjacent to or in between those of larger hydrocarbons or of other organics, only N-containing peaks whose fitting significantly reduced the residual mass at each unit mass were fit (Fig. S7). Additionally, and when possible, the w-ToF mode data was examined to determine if the N-containing peak was resolved enough from neighboring peaks for certain identification. Further discussion of this NOA factor is presented in Sect. 3.4.2.

As suggested by the relative mass contribution of m/z 57 and m/z 44 (see previous section), HOA was not the largest average contributor to the bulk measured aerosol mass over the campaign period, despite the fact that these measurements were conducted 15 m from a major highway (Fig. 9b). The relative size of each type of particle (primary, or HOA, and OOA) likely plays a major role in the relative mass concentrations of each factor. The variability of each factor over the campaign was high as, unlike measurements in more rural areas, the proximity to a primary aerosol source (highway) and to an urban center (Grenoble), as well as large green spaces (the Alps) allowed the full range of aged and locally transported aerosol to be observed at this station. The calculated elemental ratios of O : C, H : C, and N : C, along with the Organic Mass : Organic Carbon (OM : OC), (Aiken et al., 2008) are shown in Table 1. The N : C ratios are simply for qualitative reference, as the low signal of N-containing peaks and their high degree of overlap with larger oxygen-containing and hydrocarbon peaks, as well as their tendency to fragment into separate organic and nitrate peaks in the HR-ToF-AMS, makes the quantification of organic-nitrate by the HR-ToF-AMS nearly impossible in ambient data sets (Farmer et al., 2010).

ACPD
14, 27373–27424, 2014

In Fig. 10, the time series of each factor are shown with oxalate ($C_2O_4^{2-}$, a marker for aged and oxidized organic aerosol), sulfate, and levoglucosan (a marker for biomass burning) measurements from filter samples. Table 2 summarizes the R^2 values between key tracer species and the resolved aerosol factors. The BBOA factor was found to correlate with levoglucosan ($R^2 = 0.65$, $n = 38$); while significant levels of biomass burning from wood-burning stoves and other combustion-related heating are known to affect the Grenoble Valley in winter, such a large contribution during this season is surprising. Likely the PMF-resolved BBOA factor was somewhat mixed with emissions with close spectral signature (LO-OA or potentially cooking aerosol emissions), although the separation of further factors did not appear to separate cooking and biomass burning influences within the measured bulk aerosol. Episodic local yard-waste burning could also have contributed to the bulk aerosol spectrum, as spikes in the BBOA concentration do not appear to correlate with a particular wind direction (Fig. S8). The ratio of levoglucosan : BBOA is quite low (0.03); however, it is within the order of magnitude of previously reported measurements (e.g., 0.06, Aiken et al., 2009). Additionally, the higher levels of oxidants found in the atmosphere in the summer could cause a faster degradation of levoglucosan in the atmosphere after emission (Hennigan et al., 2010). Thus, the BBOA concentrations reported here shall be considered as an upper limit of the biomass burning contribution.

Oxalate and regional OOA covaried with an R^2 of 0.62 ($n = 53$). Regional OOA was identified as thus due to its low temporal variation, its correlation with SO_4, and a low correlation with wind direction (Fig. S8). This factor was removed from the atmosphere during periods of rain and experienced a slow recovery afterwards. At the beginning of the experiment (11–13 September), regional OOA and SO_4 did not correspond; however, during the middle and end of the campaign, temporal variations of the regional OOA and SO_4 corresponded fairly well ($R^2 = 0.65$, $n = 3328$). The reason for the initial high SO_4 and low regional OOA is unclear from the data set as-is; however, MO-OA and SO_4 also had similar time series trends ($R^2 = 0.50$, $n = 3328$) and MO-OA was high at the beginning of the campaign. The closeness of the two spectra's composition,

ACPD
14, 27373–27424, 2014

as well as the nature of the aerosol type (not from a specific source but rather aged bulk organic aerosol), in which variations would logically occur, may have led to the imprecise separation of these two factor types. Of the factors resolved, the HOA factor had the lowest O : C ratio (0.07) and a good ($R^2 = 0.58$, $n = 3928$) correlation with BC concentration, which suggests it was primary and from vehicular origin. The mass spectrum of the resolved HOA factor highly resembled ($R^2 > 0.95$, $n = 100$) previously resolved HOA factors and direct AMS measurements of diesel and gasoline emissions (Mohr et al., 2009; Zhang et al., 2005).

The two main factors resolved, in terms of mass concentration, were the OOA factors with opposite diurnal trends, MO-OA and LO-OA. The concentration of MO-OA rose as the aerosol number-weighted geometric mode diameter rose, also indicative of increasing aerosol age/coagulation. The LO-OA factor resembled the SV-OOA factor reported by Docherty et al. (2008) measured during the Study of Organic Aerosols (SOAR) project at Riverside, CA, which was also found to decrease during the afternoon as temperature and photochemical processing increased. Figure 11 shows the normalized difference between HOA and LO-OA (Fig. 11a) and LO-OA and MO-OA (Fig. 11b). A relative reduction in the higher-mass hydrocarbon fragments and an increase in the oxidized organic fragments are observed between HOA and LO-OA. This difference spectrum is similar to that found by Sun et al. (2012) between spectra obtained just prior to and during peaks in traffic (when the spectra would be mostly comprised of HOA). The main difference between LO-OA and MO-OA was the level of oxidation; the m/z 44 and 28 (COO^+ and CO^+, respectively) increased in MO-OA while the rest of fragments decreased in relative concentration. The increase in MO-OA concentration occurred as both PTR-MS isoprene signal was increasing (also a temperature-related process) and as the 9-carbon aromatic: benzene ($C_9H_{13}^+ : C_6H_7^+$) VOC ratio was at its minimum (related to photochemical age of air mass, Parrish et al., 2007). Thus, the increase MO-OA could be linked to photochemical aging of vehicular emissions during the day and also to increasing biogenic VOC emissions and their subsequent photochemical aging and condensation into aerosol form.

ACPD
14, 27373–27424, 2014

The PMF model was also run with unit-mass resolution (UMR) AMS data. In such a configuration, all HR factors except the NOA factor were resolved; however, the concentration of HOA rose as other species (oxidized organic peaks that share nominal masses with hydrocarbons; N-containing peaks) were folded into the HOA factor.

3.4.1 HOA : BC ratio

To better compare our HOA factor concentration and BC concentration with previously published studies, the UMR HOA factor concentration was used to calculate the concentration of HOA and a ratio of ~ 0.26 HOA : BC was found (~ 0.19 for HR HOA : BC). The comparison of the HOA : BC ratio from this study and from previously reported field studies is shown in Fig. 12. As expected, since the French fleet includes a much higher percentage of diesel cars with increased BC emissions, this ratio was significantly lower than that reported for an urban-downwind site in Pittsburgh (1.41, Zhang et al., 2005), a highway adjacent site in New York (1.02, Sun et al., 2012), an urban/highway site in Ontario (0.7–1.1, Stroud et al., 2012), a rural site in NW England (1.61–1.91, Liu et al., 2006) and an urban site in Zurich, Switzerland (1.1, Lanz et al., 2007). As for measurements in France, a study in an urban site in Paris observed a HOA : BC ratio of 0.61 (Crippa et al., 2013); this site was most probably influenced by a vehicle fleet similar to Grenoble's, but measurements were collected during winter (lower temperatures) and within Paris (increased urban emissions). Tailpipe measurements of Euro 4 diesel and gasoline-powered vehicles (a Renault Kangoo and a Ford Ka, respectively) at IFSTTAR (Institut Français des Sciences et Technologies des Transports, de l'Aménagement et des Réseaux) performed during this PM Drive research program also show a much higher HOA : BC ratio for gasoline vehicles vs. diesel vehicles (unpublished data). This was due to much higher BC emissions from the diesel vehicle, as opposed to higher HOA emissions from the gasoline vehicle. This low HOA : BC ratio in the campaign in Grenoble is in-line with reported measurements from diesel exhaust; for example, Chirico et al. (2010) found a OA : BC ratio of 0.28 in smog chamber emission (where most of the OA is likely to be "HOA-type" aerosol).

ACPD
14, 27373–27424, 2014

The HOA factor measured near Grenoble was similar to that measured by Sun et al. (2012), in a high gasoline environment next to a highway in New York, both in absolute concentration and chemical composition. The hourly traffic concentrations at each site were close (approximately 10 000 vehicles h^{-1} reported during the Sun et al. (2012) measurement periods compared to approximately 8000 vehicles h^{-1} observed during daylight driving hours in the Grenoble's highway); thus, an increase in BC emissions (from diesel) rather than a reduction in HOA : vehicle number was likely the cause of our low HOA : BC ratio. Although HDV have higher PM emission limits than LDVs for the same Euro classification, the HOA : BC ratio remained fairly steady throughout the day even as the LDV : bus/HDV ratio increased by a factor of four from morning to evening. This suggested that LDVs, rather than HDVs or buses, were more responsible for the low HOA : BC ratio and the high BC concentrations. This differs from the Sun et al. (2012) measurements. Sun et al. (2012) attribute a period of strong correlation between BC and HOA, along with a low HOA : BC ratio (of 1.02) to the influence of diesel trucks (12 %) and a day of high HOA with little to no BC due to the influence of local bus emissions powered by compressed natural gas.

Of the measurements presented in Fig. 12, the French measurement sites had by far the highest proportion of diesel vehicles and diesel fuel use. The change in HOA : BC ratio as a function of the diesel : gasoline fuel use (Road sector, World Bank, 2011) is shown in Fig. 13. A decrease in HOA : BC with an increase in percent diesel is clearly observable with a strong correlation ($R^2 = 0.85$, $n = 10$), despite the many different factors possibly influencing BC and HOA concentrations at each location (e.g., local aerosol sources, meteorology).

3.4.2 NO/NO_x/Nitrogen

High concentrations of NO_x were measured at the field site, up to 450 ppbv ($NO+NO_2$) for 15 min averaged measurements. The highest levels were recorded during the morning rush hour when the boundary layer was at its lowest, with concentrations ranging from 180–450 ppbv on different mornings. NO_2 levels exceeded the 100 ppbv European

ACPD
14, 27373–27424, 2014

hourly limit almost every morning. The campaign average for NO_2 was 94 ± 64 ppbv. For comparison, Sun et al. (2012) measured an average of 48 ± 30 ppbv NO_2, about half that of this campaign's average, with 15 min average peaks ranging from 100–300 ppbv. Since, as mentioned earlier vehicle fluxes were similar at both sites, a difference in number of vehicles cannot explain the increased amount of NO_x. Rather, increased diesel fuel use is a very likely hypothesis.

One possible effect of increased NO_x on aerosol formation is the formation of organic nitrate aerosols from the photochemical reactions of various VOC precursors in the presence of high levels of NO_x (Ng et al., 2007). During the field campaign, little evidence of typical organic nitrate peaks (e.g., CH_4NO, C_2H_5NO, C_3H_4NO, CH_2NO_3, CH_2NO_2, Farmer et al., 2010) was found in the high resolution mass spectra. In low concentrations, organic nitrates are difficult to observe in the HR-ToF-AMS as the high energy of ionization (70 eV) used to ionize molecules in the HR-ToF-AMS likely causes most organic nitrate to fragment into organic species and nitrate species in the mass spectra (Farmer et al., 2010). Deviations of the $NO_{aero} : NO_{2aero}$ ratio (m/z 30 and m/z 46, respectively) from the inorganic nitrate ratio of these two mass fragments in the measured HR-ToF-AMS spectra has been proposed to indicate the presence or absence of organic nitrate (Bruns et al., 2010; Farmer et al., 2010; Fry et al., 2013). Note that, in this paragraph, NO_{aero} and NO_{2aero} refer to peaks in the aerosol mass spectra, not gas-phase NO_x. Individual instrument tuning and sensitivity can change the ratio of NO and NO_2; however, the ratio should remain the same throughout a measurement period for inorganic nitrate (Farmer et al., 2010). During the campaign, the aerosol NO_{aero}: NO_{2aero} ratio was about 4.6 when the best-fit line was forced through the origin. This ratio varied throughout the day: from midday to evening, when temperatures and photolysis rates were highest, the bulk aerosol NO_{aero}: NO_{2aero} ratio was greater than 4.6 (Fig. 14). This peak in the NO_{aero}: NO_{2aero} ratio corresponded to a daily dip in the aerosol nitrate concentration (although still greater than the limit of detection of 0.06) and to the peak solar hours, which suggests that organic nitrates, if present,

ACPD
14, 27373–27424, 2014

were likely both small contributors to the total nitrate measured and also formed from photochemical processing, not directly emitted by vehicles.

In addition, the N-containing peaks within the spectrum of the NOA factor contained mostly amine-like fragments and had a diurnal pattern that was not correlated to changes in the $NO_{aero} : NO_{2aero}$ ratio; thus, the NOA factor resolved was likely not composed of organic nitrates but rather composed of amine-containing organic species. Saarikoski et al. (2012) found a similar amine-containing NOA factor in measurements taken in the Po Valley (Italy) that also had a strong diurnal pattern. However, their NOA factor was attributed to marine influence due to a correlation with MSA (Saarikoski et al., 2012), although it is possible that MSA was from the local industrial use of DMSO as a solvent, and had a higher H : C ratio (1.91) than the factor resolved from this data set (1.38). Aiken et al. (2009) and Sun et al. (2011) also resolved N-containing OA factors from data measured in Mexico City and New York, respectively, but did not observe a similar diurnal pattern in N-containing aerosol concentration.

In the PTR-MS mass spectra results obtained from Euro 5 vehicle emission smog chamber studies, Hellebust et al. (2014, 2013) found higher nitrogen-containing emissions from fresh and aged diesel mass than from fresh and aged gasoline mass spectra (e.g., peaks such as $CH_4NO_2^+$). Similar nitrogen-containing VOC peaks were found by Inomata et al. (2013) in diesel exhaust. Also, fresh and aged diesel VOC emissions had higher relative levels of oxygen than fresh gasoline emissions (Hellebust et al., 2014). The O : C ratio of the NOA factor was calculated to be 0.4, greater than the 0.07 O : C ratio calculated for the HOA factor spectrum. Russell et al. (2011) identified small but constant concentrations of amines from aerosol measured in a variety of environments and attributed these amines, in part, to combustion processes. Thus, diesel-related emissions could possibly be the source for the observed NOA factor. During the campaign, the calculated NOA factor and measured BC (BC most likely due to diesel emissions) had no significant ($R^2 = 0.09$, $n = 3926$) correlation. Thus, while the NOA factor resolved temporally resembled a traffic-related emission, it is not definitively linked to traffic emission tracers. Therefore, its exact source is difficult to determine. Possibly

ACPD
14, 27373–27424, 2014

the NOA factor represents the rapid formation of semi-volatile SOA from diesel VOC emissions, but the different lifetimes of VOCs vs. aerosol, and the issue of transport and aging for SOA formation, would make this difficult to definitively determine.

3.5 Fossil and modern carbon

To discriminate between the relative influence of modern and fossil carbon at the sampling site, daily filter samples were collected and C-14 radiocarbon measurements were performed. From these measurements, the percentage of modern carbon (from the sum of both OC and EC) was calculated. Modern carbon varied from 15–36 % of the total aerosol carbon, a significant portion of the measured carbon considering the close proximity of the measurements to fossil carbon sources. In France, the contribution of biofuel were about 7 and 5 % for diesel and gasoline, respectively, in 2011 (UFIP, Union Française des Industries Petrolières, 2011) and cannot explain this relative high proportion of modern carbon observed in the particulate matter. This is similar to findings shown in Hodzic et al. (2010), Minguillon et al. (2011), and El Haddad et al. (2013), which indicate that modern carbon is often more significant than fossil carbon in the carbonaceous fraction of PM, even in cities with high vehicular emissions (e.g., Mexico City, Barcelona or Marseille).

Assuming that the majority of BC was traffic-related, and thus from fossil origin, the concentration of modern organic carbon and fossil organic carbon was then calculated. While evidence for the presence of biomass burning aerosol was measured at the field site, the main source of BC was likely diesel exhaust. The concentration of BBOA was generally low (a campaign average of $0.34 \pm 0.23\,\mu g\,m^{-3}$) and the ratio of BBOA : BC has been found to be on the order of 3–4 in other areas of France (Crippa et al., 2013), the combination of which would make a BBOA contribution to BC fairly negligible during our study. Figure 15 shows the fraction of black carbon, modern organic carbon, fossil organic carbon, and HOA as a function of total carbon mass (OC + BC). The HOA factor concentration has been divided by its OM : OC ratio to remove any non-carbon

ACPD
14, 27373–27424, 2014

mass (calculated from the elemental formulas of the PMF factor mass spectra, Aiken et al., 2008).

Total organic carbon concentration appeared to be more driven by processed/aged OOA concentrations than by primary emissions. During the period with the highest organic concentrations (15–17 September), most of the non-HOA carbon measured was modern carbon. At other times during the campaign, HOA concentrations alone could not adequately explain all of the measured fossil organic carbon and additional sources of fossil organic carbon (such as photochemical reactions forming aerosol from vehicular VOC emissions) would be needed. Overall, throughout the campaign the majority of SOA observed was most probably from modern origin.

The large fraction of OOA within the overall mass spectra, especially the presence of the MO-OA factor increasing during times of high photochemical processing potential, suggested that photochemically aged aerosol were more important to the daily aerosol mass concentration than primary emissions at the measurement site. Additionally, the high levels of modern carbon SOA suggested that biogenic compounds had the greatest effect on the overall aerosol population in this location, even directly next to a large anthropogenic emission source (i.e., traffic). However, the interaction between anthropogenic oxidants and biogenic VOCs (or BVOCs) has been found to increase the formation of SOA (Chameides et al., 1988; Goldstein et al., 2009; Shilling et al., 2013). Isoprene oxidation reactions leading towards SOA have been shown to vary depending on the level of NO_x (Chen et al., 2014; Kroll et al., 2005; Ng et al., 2007; Xu et al., 2014). Although BVOC concentrations and aromatic VOC concentrations were similar in magnitude throughout the campaign (few ppbv), and the isoprene/NO_x ratio was low at the measurement site (less than 0.01), likely BVOC concentrations were greater and the aromatic VOC concentrations were lower in the wider Grenoble Valley. Aerosol transport and the influence of anthropogenic oxidants from vehicular emissions on overall aerosol formation and concentration could both have influenced the aerosol population measured during this campaign.

ACPD
14, 27373–27424, 2014

4 Conclusions

During this campaign, highly time resolved particle and gas-phase chemical composition and concentration measurements were obtained alongside parallel traffic data of the speed, fluxes, vehicle type, and fuel type of passing cars on a highway in the Grenoble Valley. A complete analysis of the local primary (traffic) aerosol and the more regional, aged secondary organic aerosol was performed for the PM_1 fraction observed by the HR-ToF-AMS. The PMF model was run on the high-resolution HR-ToF-AMS aerosol data and six factors were resolved from the bulk aerosol data: (1) an HOA factor, related to traffic (2) a BBOA factor (3) a regional OOA factor, which covaried with sulfate (4) a MO-OA factor, increasing in concentration during sunny afternoons (5) a LO-OA factor, with the opposite diurnal pattern as MO-OA, likely due to gas-particle phase partitioning and photochemical processing and (6) an NOA factor with a diurnal pattern similar to that of HOA and to traffic peaks.

The resolved mass spectrum for the HOA factor was chemically similar to mass spectra from both gasoline and diesel-emitted organic carbon and previously resolved HOA factors in high-gasoline environments; however, the HOA : BC ratio measured was low (< 0.3) throughout the campaign. This ratio agrees with previously reported HOA : BC ratios in high diesel environments and from direct measurements of diesel emissions in smog chamber and tailpipe measurement studies. The fraction of diesel-powered vehicles on the road appeared to control, to some extent, this ratio. Periods of heavy traffic were associated with both increased HOA and BC along with increased particle number concentration and lower particle size. While high levels of both black carbon ($5 \pm 3\,\mu g\,m^{-3}$) and organic aerosol ($8 \pm 4\,\mu g\,m^{-3}$) were measured, when examined, only 20 % of the total organic mass signal could be attributed to primary vehicular emissions (i.e., HOA). Traffic emissions dominated the aerosol particle number concentration, but the majority of the organic aerosol mass concentration measured was SOA. NO_x concentrations in these measurements were two times higher than concentrations near a similarly-trafficked highway in New York, USA. Although NO_x and VOCs emitted by

ACPD
14, 27373–27424, 2014

diesel and gasoline engines, respectively, may have influenced SOA formation in the Grenoble Valley, the majority of SOA measured was modern in origin, even adjacent to a major source of fossil carbon. Whether this is due to a lower overall gas+particle emission of diesel vehicles, the lack of aromatic compounds in diesel VOC emissions, high NO_x reducing the efficiency of vehicular VOC to SOA formation mechanisms, an acceleration of BVOC to biogenic aerosol formation in the presence of vehicular emissions, or simply the more global source and higher efficiency of BVOC to SOA reactions is unclear, but in a high diesel environment, SOA from fossil-fuel carbon was only a small source of the measured OOA, while OOA dominated the carbonaceous aerosol mass in the fine fraction of PM_1.

The Supplement related to this article is available online at doi:10.5194/acpd-14-27373-2014-supplement.

Acknowledgements. This work was supported by the French Environment and Energy Management Agency (ADEME, Grant number 1162C0002). The authors gratefully acknowledge the NOAA Air Resources Laboratory (ARL) for the provision of the HYSPLIT transport and dispersion model (http://www.ready.noaa.gov) used in this publication. We also gratefully acknowledge Air Rhone Alpes staff (particularly Yann Pellan) for their support during the campaign as well as Y. Sun and Q. Zhang for providing near-highway aerosol data from their paper Sun et al. (2012) for comparison with these measurements.

Finally, the authors gratefully acknowledge the MASSALYA instrumental platform (Aix Marseille Université, lce.univ-amu.fr) for the analysis and measurements used in this publication.

References

Aiken, A. C., Salcedo, D., Cubison, M. J., Huffman, J. A., DeCarlo, P. F., Ulbrich, I. M., Docherty, K. S., Sueper, D., Kimmel, J. R., Worsnop, D. R., Trimborn, A., Northway, M., Stone, E. A., Schauer, J. J., Volkamer, R. M., Fortner, E., de Foy, B., Wang, J., Laskin, A.,

ACPD
14, 27373–27424, 2014

Shutthanandan, V., Zheng, J., Zhang, R., Gaffney, J., Marley, N. A., Paredes-Miranda, G., Arnott, W. P., Molina, L. T., Sosa, G., and Jimenez, J. L.: Mexico City aerosol analysis during MILAGRO using high resolution aerosol mass spectrometry at the urban supersite (T0) – Part 1: Fine particle composition and organic source apportionment, Atmos. Chem. Phys., 9, 6633–6653, doi:10.5194/acp-9-6633-2009, 2009.

Aiken, A. C., Decarlo, P. F., Kroll, J. H., Worsnop, D. R., Huffman, J. A., Docherty, K. S., Ulbrich, I. M., Mohr, C., Kimmel, J. R., Sueper, D., Sun, Y., Zhang, Q., Trimborn, A., Northway, M., Ziemann, P. J., Canagaratna, M. R., Onasch, T. B., Alfarra, M. R., Prevot, A. S. H., Dommen, J., Duplissy, J., Metzger, A., Baltensperger, U., and Jimenez, J. L.: O/C and OM/OC ratios of primary, secondary, and ambient organic aerosols with high-resolution time-of-flight aerosol mass spectrometry, Environ. Sci. Technol., 42, 4478–4485, 2008.

Bahreini, R., Middlebrook, A. M., de Gouw, J. A., Warneke, C., Trainer, M., Brock, C. A., Stark, H., Brown, S. S., Dube, W. P., Gilman, J. B., Hall, K., Holloway, J. S., Kuster, W. C., Perring, A. E., Prevot, A. S. H., Schwarz, J. P., Spackman, J. R., Szidat, S., Wagner, N. L., Weber, R. J., Zotter, P., and Parrish, D. D.: Gasoline emissions dominate over diesel in formation of secondary organic aerosol mass, Geophys. Res. Lett., 39, doi:10.1029/2011GL050718, 2012.

Birch, M. E. and Cary, R. A.: Elemental carbon-based method for monitoring occupational exposures to particulate diesel exhaust, Aerosol Sci. Tech., 25, 221–241, 1996.

Bond, T. C., Doherty, S. J., Fahey, D. W., Forster, P. M., Berntsen, T., DeAngelo, B. J., Flanner, M. G., Ghan, S., Kärcher, B., Koch, D., Kinne, S., Kondo, Y., Quinn, P. K., Sarofim, M. C., Schultz, M. G., Schulz, M., Venkataraman, C., Zhang, H., Zhang, S., Bellouin, N., Guttikunda, S. K., Hopke, P. K., Jacobson, M. Z., Kaiser, J. W., Klimont, Z., Lohmann, U., Schwarz, J. P., Shindell, D., Storelvmo, T., Warren, S. G., and Zender, C. S.: Bounding the role of black carbon in the climate system: a scientific assessment, J. Geophys. Res.-Atmos., 118, 5380–5552, doi:10.1002/jgrd.50171, 2013.

Broderick, B. and Marnane, I.: A comparison of the C2–C9 hydrocarbon compositions of vehicle fuels and urban air in Dublin, Ireland, Atmos. Environ., 36, 975–986, doi:10.1016/S1352-2310(01)00472-1, 2002.

Brugge, D., Durant, J. L., and Rioux, C.: Near-highway pollutants in motor vehicle exhaust: a review of epidemiologic evidence of cardiac and pulmonary health risks, Environ. Health, 6, 23, doi:10.1186/1476-069X-6-23, 2007.

ACPD
14, 27373–27424, 2014

Bruns, E. A, Perraud, V., Zelenyuk, A., Ezell, M. J., Johnson, S. N., Yu, Y., Imre, D., Finlayson-Pitts, B. J., and Alexander, M. L.: Comparison of FTIR and particle mass spectrometry for the measurement of particulate organic nitrates., Environ. Sci. Technol., 44, 1056–61, doi:10.1021/es9029864, 2010.

Carlton, A. G., Wiedinmyer, C., and Kroll, J. H.: A review of Secondary Organic Aerosol (SOA) formation from isoprene, Atmos. Chem. Phys., 9, 4987–5005, doi:10.5194/acp-9-4987-2009, 2009.

Cavalli, F., Viana, M., Yttri, K. E., Genberg, J., and Putaud, J.-P.: Toward a standardised thermal-optical protocol for measuring atmospheric organic and elemental carbon: the EUSAAR protocol, Atmos. Meas. Tech., 3, 79–89, doi:10.5194/amt-3-79-2010, 2010.

Chameides, W., Lindsay, R., Richardson, J., and Kiang, C.: The role of biogenic hydrocarbons in urban photochemical smog: atlanta as a case study, Science, 241, 1473–1475, doi:10.1126/science.3420404, 1988.

Chen, J., Zhao, C. S., Ma, N., and Yan, P.: Aerosol hygroscopicity parameter derived from the light scattering enhancement factor measurements in the North China Plain, Atmos. Chem. Phys., 14, 8105–8118, doi:10.5194/acp-14-8105-2014, 2014.

Chirico, R., DeCarlo, P. F., Heringa, M. F., Tritscher, T., Richter, R., Prévôt, A. S. H., Dommen, J., Weingartner, E., Wehrle, G., Gysel, M., Laborde, M., and Baltensperger, U.: Impact of aftertreatment devices on primary emissions and secondary organic aerosol formation potential from in-use diesel vehicles: results from smog chamber experiments, Atmos. Chem. Phys., 10, 11545–11563, doi:10.5194/acp-10-11545-2010, 2010.

Crippa, M., DeCarlo, P. F., Slowik, J. G., Mohr, C., Heringa, M. F., Chirico, R., Poulain, L., Freutel, F., Sciare, J., Cozic, J., Di Marco, C. F., Elsasser, M., Nicolas, J. B., Marchand, N., Abidi, E., Wiedensohler, A., Drewnick, F., Schneider, J., Borrmann, S., Nemitz, E., Zimmermann, R., Jaffrezo, J.-L., Prévôt, A. S. H., and Baltensperger, U.: Wintertime aerosol chemical composition and source apportionment of the organic fraction in the metropolitan area of Paris, Atmos. Chem. Phys., 13, 961–981, doi:10.5194/acp-13-961-2013, 2013.

Decarlo, P. F., Kimmel, J. R., Trimborn, A., Northway, M. J., Jayne, J. T., Aiken, A. C., Gonin, M., Fuhrer, K., Horvath, T., Docherty, K. S., Worsnop, D. R., and Jimenez, J. L.: Field-deployable, high-resolution, time-of-flight aerosol mass spectrometer, Anal. Chem., 78, 8281–8289, doi:10.1021/ac061249n, 2006.

Docherty, K. S., Stone, E. A., Ulbrich, I. M., DeCarlo, P. F., Snyder, D. C., Schauer, J. J., Peltier, R. E., Weber, R. J., Murphy, S. M., Seinfeld, J. H., Grover, B. D., Eatough, D. J.,

ACPD
14, 27373–27424, 2014

and Jimenez, J. L.: Apportionment of primary and secondary organic aerosols in southern California during the 2005 Study of Organic Aerosols in Riverside (SOAR-1), Environ. Sci. Technol., 42, 7655–7662, doi:10.1021/es8008166, 2008.

El Haddad, I., Marchand, N., Dron, J., Temime-Roussel, B., Quivet, E., Wortham, H., Jaffrezo, J. L., Baduel, C., Voisin, D., Besombes, J. L., and Gille, G.: Comprehensive primary particulate organic characterization of vehicular exhaust emissions in France, Atmos. Environ., 43, 6190–6198, doi:10.1016/j.atmosenv.2009.09.001, 2009.

El Haddad, I., Marchand, N., Wortham, H., Piot, C., Besombes, J.-L., Cozic, J., Chauvel, C., Armengaud, A., Robin, D., and Jaffrezo, J.-L.: Primary sources of $PM_{2.5}$ organic aerosol in an industrial Mediterranean city, Marseille, Atmos. Chem. Phys., 11, 2039–2058, doi:10.5194/acp-11-2039-2011, 2011.

El Haddad, I., D'Anna, B., Temime-Roussel, B., Nicolas, M., Boreave, A., Favez, O., Voisin, D., Sciare, J., George, C., Jaffrezo, J.-L., Wortham, H., and Marchand, N.: Towards a better understanding of the origins, chemical composition and aging of oxygenated organic aerosols: case study of a Mediterranean industrialized environment, Marseille, Atmos. Chem. Phys., 13, 7875–7894, doi:10.5194/acp-13-7875-2013, 2013.

Farmer, D. K., Matsunaga, A., Docherty, K. S., Surratt, J. D., Seinfeld, J. H., Ziemann, P. J., and Jimenez, J. L.: Response of an aerosol mass spectrometer to organonitrates and organosulfates and implications for atmospheric chemistry, P. Natl. Acad. Sci. USA, 107, 6670–6675, doi:10.1073/pnas.0912340107, 2010.

Favez, O., El Haddad, I., Piot, C., Boréave, A., Abidi, E., Marchand, N., Jaffrezo, J.-L., Besombes, J.-L., Personnaz, M.-B., Sciare, J., Wortham, H., George, C., and D'Anna, B.: Intercomparison of source apportionment models for the estimation of wood burning aerosols during wintertime in an Alpine city (Grenoble, France), Atmos. Chem. Phys., 10, 5295–5314, doi:10.5194/acp-10-5295-2010, 2010.

Fry, J. L., Draper, D. C., Zarzana, K. J., Campuzano-Jost, P., Day, D. A., Jimenez, J. L., Brown, S. S., Cohen, R. C., Kaser, L., Hansel, A., Cappellin, L., Karl, T., Hodzic Roux, A., Turnipseed, A., Cantrell, C., Lefer, B. L., and Grossberg, N.: Observations of gas- and aerosol-phase organic nitrates at BEACHON-RoMBAS 2011, Atmos. Chem. Phys., 13, 8585–8605, doi:10.5194/acp-13-8585-2013, 2013.

Gentner, D. R., Isaacman, G., Worton, D. R., Chan, A. W. H., Dallmann, T. R., Davis, L., Liu, S., Day, D. A, Russell, L. M., Wilson, K. R., Weber, R., Guha, A., Harley, R. A. and Goldstein, A. H.: Elucidating secondary organic aerosol from diesel and gasoline vehicles

ACPD
14, 27373–27424, 2014

through detailed characterization of organic carbon emissions, P. Natl. Acad. Sci. USA, 109, 18318–18323, doi:10.1073/pnas.1212272109, 2012.
Goldstein, A. H., Koven, C. D., Heald, C. L., and Fung, I. Y.: Biogenic carbon and anthropogenic pollutants combine to form a cooling haze over the southeastern United States, P. Natl. Acad. Sci. USA, 106, 8835–8840, doi:10.1073/pnas.0904128106, 2009.
Hellebust, S., Temime-Roussel, B., Bertrand, A., Platt, S. M., El Haddad, I., Pieber, S., Zardini, A. A., Suarez-Bertoa, R., Slowik, J. G., Huang, R. J., Astorga, C., Prevot, A. S. H., and Marchand, N.: Comparison of gasoline and diesel vehicles-emission factors of volatile organic compounds from EURO5 diesel and gasoline vehicles and their potential integrated influence on air quality, Am. Assoc. Aerosol Res., 2013.
Hellebust, S., Temime-Roussel, B., Bertrand, A., Platt, S. M., El Haddad, I., Pieber, S., Zardini, A. A., Suarez-Bertoa, R., Slowik, J. G., Huang, R. J., Astorga, C., Prevot, A. S. H., and Marchand, N.: Emission Factors of Volatile Organic Compounds measured by Proton Transfer Reaction – Time-of-Flight – Mass Spectrometry 1. Euro 2 Scooter, Euro 5 Light Duty Gasoline and Diesel Vehicles and Euro V Heavy Duty Diesel Vehicles, in preparation, 2014.
Hennigan, C. J., Sullivan, A. P., Collett, J. L., and Robinson, A. L.: Levoglucosan stability in biomass burning particles exposed to hydroxyl radicals, Geophys. Res. Lett., 37, doi:10.1029/2010GL043088, 2010.
Herich, H., Gianini, M. F. D., Piot, C., Moènik, G., Jaffrezo, J.-L., Besombes, J.-L., Prévôt, A. S. H., and Hueglin, C.: Overview of the impact of wood burning emissions on carbonaceous aerosols and PM in large parts of the Alpine region, Atmos. Environ., 89, 64–75, doi:10.1016/j.atmosenv.2014.02.008, 2014.
Hodzic, A., Jimenez, J. L., Madronich, S., Canagaratna, M. R., DeCarlo, P. F., Kleinman, L., and Fast, J.: Modeling organic aerosols in a megacity: potential contribution of semi-volatile and intermediate volatility primary organic compounds to secondary organic aerosol formation, Atmos. Chem. Phys., 10, 5491–5514, doi:10.5194/acp-10-5491-2010, 2010.
Huffman, J. A., Jayne, J. T., Drewnick, F., Aiken, A. C., Onasch, T., Worsnop, D. R., and Jimenez, J. L.: Design, modeling, optimization, and experimental tests of a particle beam width probe for the aerodyne aerosol mass spectrometer, Aerosol Sci. Tech., 39, 1143–1163, doi:10.1080/02786820500423782, 2005.
Hyvärinen, A.-P., Vakkari, V., Laakso, L., Hooda, R. K., Sharma, V. P., Panwar, T. S., Beukes, J. P., van Zyl, P. G., Josipovic, M., Garland, R. M., Andreae, M. O., Pöschl, U., and Petzold, A.: Correction for a measurement artifact of the Multi-Angle Absorption Photome-

ACPD
14, 27373–27424, 2014

ter (MAAP) at high black carbon mass concentration levels, Atmos. Meas. Tech., 6, 81–90, doi:10.5194/amt-6-81-2013, 2013.
Inomata, S., Tanimoto, H., Fujitani, Y., Sekimoto, K., Sato, K., Fushimi, A., Yamada, H., Hori, S., Kumazawa, Y., Shimono, A., and Hikida, T.: On-line measurements of gaseous nitro-organic compounds in diesel vehicle exhaust by proton-transfer-reaction mass spectrometry, Atmos. Environ., 73, 195–203, doi:10.1016/j.atmosenv.2013.03.035, 2013.
Jaffrezo, J. L., Davidson, C. I., Kuhns, H. D., Bergin, M. H., Hillamo, R., Maenhaut, W., Kahl, J. W., and Harris, J. M.: Biomass burning signatures in the atmosphere of central Greenland, J. Geophys. Res.-Atmos., 103, doi:10.1029/98JD02241, 31067–31078, 1998.
Jaffrezo, J.-L., Aymoz, G., and Cozic, J.: Size distribution of EC and OC in the aerosol of Alpine valleys during summer and winter, Atmos. Chem. Phys., 5, 2915–2925, doi:10.5194/acp-5-2915-2005, 2005.
Janssen, N. A. H.: World Health Organization, Regional Office for Europe and Joint WHO/Convention Task Force on the Health Aspects of Air Pollution: Health Effects of Black Carbon, available at: http://www.euro.who.int/__data/assets/pdf_file/0004/162535/e96541.pdf, 2012.
Kroll, J. H., Ng, N. L., Murphy, S. M., Flagan, R. C., and Seinfeld, J. H.: Secondary organic aerosol formation from isoprene photooxidation under high-NO_x conditions, Geophys. Res. Lett., 32, doi:10.1029/2005GL023637, 2005.
Lanz, V. A., Alfarra, M. R., Baltensperger, U., Buchmann, B., Hueglin, C., and Prévôt, A. S. H.: Source apportionment of submicron organic aerosols at an urban site by factor analytical modelling of aerosol mass spectra, Atmos. Chem. Phys., 7, 1503–1522, doi:10.5194/acp-7-1503-2007, 2007.
Lighty, J. S., Veranth, J. M., and Sarofim, A. F.: Combustion aerosols: factors governing their size and composition and implications to human health, J. Air Waste Manage., 50, 1565–1618, doi:10.1080/10473289.2000.10464197, 2000.
Liu, L., Lacis, A. A., Carlson, B. E., Mishchenko, M. I., and Cairns, B.: Assessing Goddard Institute for Space Studies ModelE aerosol climatology using satellite and ground-based measurements: a comparison study, J. Geophys. Res., 111, D20212, doi:10.1029/2006JD007334, 2006.
Matthew, B. M., Middlebrook, A. M., and Onasch, T. B.: Collection efficiencies in an aerodyne aerosol mass spectrometer as a function of particle phase for laboratory generated aerosols, Aerosol Sci. Tech., 42, 884–898, doi:10.1080/02786820802356797, 2008.

ACPD
14, 27373–27424, 2014

Minguillón, M. C., Perron, N., Querol, X., Szidat, S., Fahrni, S. M., Alastuey, A., Jimenez, J. L., Mohr, C., Ortega, A. M., Day, D. A., Lanz, V. A., Wacker, L., Reche, C., Cusack, M., Amato, F., Kiss, G., Hoffer, A., Decesari, S., Moretti, F., Hillamo, R., Teinilä, K., Seco, R., Peñuelas, J., Metzger, A., Schallhart, S., Müller, M., Hansel, A., Burkhart, J. F., Baltensperger, U., and Prévôt, A. S. H.: Fossil versus contemporary sources of fine elemental and organic carbonaceous particulate matter during the DAURE campaign in Northeast Spain, Atmos. Chem. Phys., 11, 12067–12084, doi:10.5194/acp-11-12067-2011, 2011.

Mohr, C., Huffman, J. A., Cubison, M. J., Aiken, A. C., Kenneth, S., Kimmel, J. R., Ulbrich, I. M., Hannigan, M., and Jimenez, J. L.: Characterization of primary organic aerosol emissions from meat cooking, trash burning, and motor vehicles with high-resolution aerosol mass spectrometry and comparison with ambient and chamber observations characterization of primary organic aerosol, Environ. Sci. Tech., 103, 31067–31078, doi:10.1029/98JD02241, 2009.

Ng, N. L., Kroll, J. H., Chan, A. W. H., Chhabra, P. S., Flagan, R. C., and Seinfeld, J. H.: Secondary organic aerosol formation from *m*-xylene, toluene, and benzene, Atmos. Chem. Phys., 7, 3909–3922, doi:10.5194/acp-7-3909-2007, 2007.

Ng, N. L., Kwan, A. J., Surratt, J. D., Chan, A. W. H., Chhabra, P. S., Sorooshian, A., Pye, H. O. T., Crounse, J. D., Wennberg, P. O., Flagan, R. C., and Seinfeld, J. H.: Secondary organic aerosol (SOA) formation from reaction of isoprene with nitrate radicals (NO_3), Atmos. Chem. Phys., 8, 4117–4140, doi:10.5194/acp-8-4117-2008, 2008.

Nordin, E. Z., Eriksson, A. C., Roldin, P., Nilsson, P. T., Carlsson, J. E., Kajos, M. K., Hellén, H., Wittbom, C., Rissler, J., Löndahl, J., Swietlicki, E., Svenningsson, B., Bohgard, M., Kulmala, M., Hallquist, M., and Pagels, J. H.: Secondary organic aerosol formation from idling gasoline passenger vehicle emissions investigated in a smog chamber, Atmos. Chem. Phys., 13, 6101–6116, doi:10.5194/acp-13-6101-2013, 2013.

Parrish, D. D., Stohl, A., Forster, C., Atlas, E. L., Blake, D. R., Goldan, P. D., Kuster, W. C., and de Gouw, J. A.: Effects of mixing on evolution of hydrocarbon ratios in the troposphere, J. Geophys. Res.-Atmos., 112, doi:10.1029/2006JD007583, 2007.

Platt, S. M., El Haddad, I., Zardini, A. A., Clairotte, M., Astorga, C., Wolf, R., Slowik, J. G., Temime-Roussel, B., Marchand, N., Ježek, I., Drinovec, L., Močnik, G., Möhler, O., Richter, R., Barmet, P., Bianchi, F., Baltensperger, U., and Prévôt, A. S. H.: Secondary organic aerosol formation from gasoline vehicle emissions in a new mobile environmental reaction chamber, Atmos. Chem. Phys., 13, 9141–9158, doi:10.5194/acp-13-9141-2013, 2013.

ACPD
14, 27373–27424, 2014

Polo-Rehn, L.: Caractérisation des Polluants dus au Transport Routier?: Apports Méthodologiques et Cas d'Études en Rhône Alpes, Ph.D. thesis, Grenoble Univ., 2013.
Presto, A. A., Miracolo, M. A., Donahue, N. M., and Robinson, A. L.: Secondary organic aerosol formation from high-NO_x photo-oxidation of low volatility precursors: n-alkanes, Environ. Sci. Technol., 44, 2029–2034, doi:10.1021/es903712r, 2010.
Russell, L. M., Bahadur, R., and Ziemann, P. J.: Identifying organic aerosol sources by comparing functional group composition in chamber and atmospheric particles, P. Natl. Acad. Sci. USA, 108, 3516–3521, doi:10.1073/pnas.1006461108, 2011.
Saarikoski, S., Carbone, S., Decesari, S., Giulianelli, L., Angelini, F., Canagaratna, M., Ng, N. L., Trimborn, A., Facchini, M. C., Fuzzi, S., Hillamo, R., and Worsnop, D.: Chemical characterization of springtime submicrometer aerosol in Po Valley, Italy, Atmos. Chem. Phys., 12, 8401–8421, doi:10.5194/acp-12-8401-2012, 2012.
Shilling, J. E., Zaveri, R. A., Fast, J. D., Kleinman, L., Alexander, M. L., Canagaratna, M. R., Fortner, E., Hubbe, J. M., Jayne, J. T., Sedlacek, A., Setyan, A., Springston, S., Worsnop, D. R., and Zhang, Q.: Enhanced SOA formation from mixed anthropogenic and biogenic emissions during the CARES campaign, Atmos. Chem. Phys., 13, 2091–2113, doi:10.5194/acp-13-2091-2013, 2013.
Stroud, C. A., Moran, M. D., Makar, P. A., Gong, S., Gong, W., Zhang, J., Slowik, J. G., Abbatt, J. P. D., Lu, G., Brook, J. R., Mihele, C., Li, Q., Sills, D., Strawbridge, K. B., McGuire, M. L., and Evans, G. J.: Evaluation of chemical transport model predictions of primary organic aerosol for air masses classified by particle component-based factor analysis, Atmos. Chem. Phys., 12, 8297–8321, doi:10.5194/acp-12-8297-2012, 2012.
Sun, Y. L., Zhang, Q., Schwab, J. J., Chen, W.-N., Bae, M.-S., Hung, H.-M., Lin, Y.-C., Ng, N. L., Jayne, J., Massoli, P., Williams, L. R., and Demerjian, K. L.: Characterization of near-highway submicron aerosols in New York City with a high-resolution aerosol mass spectrometer, Atmos. Chem. Phys., 12, 2215–2227, doi:10.5194/acp-12-2215-2012, 2012.
Sun, Y., Zhang, Q., Zheng, M., Ding, X., Edgerton, E. S., and Wang, X.: Characterization and source apportionment of water-soluble organic matter in atmospheric fine particles ($PM_{2.5}$) with high-resolution aerosol mass spectrometry and GC-MS., Environ. Sci. Technol., 45, 4854–4861, doi:10.1021/es200162h, 2011.
Thornhill, D. A., Williams, A. E., Onasch, T. B., Wood, E., Herndon, S. C., Kolb, C. E., Knighton, W. B., Zavala, M., Molina, L. T., and Marr, L. C.: Application of positive matrix factorization to on-road measurements for source apportionment of diesel- and gasoline-powered

ACPD
14, 27373–27424, 2014

vehicle emissions in Mexico City, Atmos. Chem. Phys., 10, 3629–3644, doi:10.5194/acp-10-3629-2010, 2010.
Ulbrich, I. M., Canagaratna, M. R., Zhang, Q., Worsnop, D. R., and Jimenez, J. L.: Interpretation of organic components from Positive Matrix Factorization of aerosol mass spectrometric data, Atmos. Chem. Phys., 9, 2891–2918, doi:10.5194/acp-9-2891-2009, 2009.
Vestreng, V., Ntziachristos, L., Semb, A., Reis, S., Isaksen, I. S. A., and Tarrasón, L.: Evolution of NO_x emissions in Europe with focus on road transport control measures, Atmos. Chem. Phys., 9, 1503–1520, doi:10.5194/acp-9-1503-2009, 2009.
WHO: Health Effects of Particulate Matter: Policy Imlications For Countries in Eastern Europe, Caucasus and Central Asia, World Health Organ., 15, available at: www.euro.who.int, 2013.
World Bank: World Development Report 2011: World Development Indicators, Fossil Fuel Energy Consumption, 2011.
Xu, J., Zhang, Q., Chen, M., Ge, X., Ren, J., and Qin, D.: Chemical composition, sources, and processes of urban aerosols during summertime in Northwest China: insights from High Resolution Aerosol Mass Spectrometry, Atmos. Chem. Phys. Discuss., 14, 16187–16242, doi:10.5194/acpd-14-16187-2014, 2014.
Zhang, Q., Worsnop, D. R., Canagaratna, M. R., and Jimenez, J. L.: Hydrocarbon-like and oxygenated organic aerosols in Pittsburgh: insights into sources and processes of organic aerosols, Atmos. Chem. Phys., 5, 3289–3311, doi:10.5194/acp-5-3289-2005, 2005.

ACPD
14, 27373–27424, 2014

Table 1. Elemental ratios of PMF-resolved factors (Aiken et al., 2008).

PMF FACTOR	OM : OC	H : C	O : C	N : C[1]
HOA	1.25	1.89	0.07	0.002
NOA	1.69	1.38	0.4	0.028
LO-OA	1.74	1.34	0.47	0.005
MO-OA	2.15	1.16	0.78	0.001
BBOA	1.56	1.47	0.32	0.01
OOA-REG	1.85	1.54	0.52	0.0006

[1] N : C ratio is not quantitative and is only shown to illustrate potential presence of nitrogen-containing organic aerosol in each factor.

ACPD
14, 27373–27424, 2014

Table 2. Correlation coefficients between PMF-resolved factors and tracer species.

PMF factor	Oxalate (N = 53) R^2	BC[a] (N = 3928) R^2	Levoglucosan (N = 38) R^2	Sulfate (N = 3328)[b] R^2
HOA	0.01	0.58	0.12	0.004
BBOA	0.04	0.05	0.65	0.005
MO-OA	0.50	0.01	0.02	0.54
LO-OA	0.32	0.01	0.08	0.07
NOA	0.01	0.09	0.12	0.06
OOA-REG	0.62	0.02	0.01	0.65

[a] BC data smoothed to remove underestimated BC concentrations during periods of high filter loading (Hyvärinen et al., 2013).
[b] R^2 value calculated after initial high SO_4 period.

ACPD
14, 27373–27424, 2014

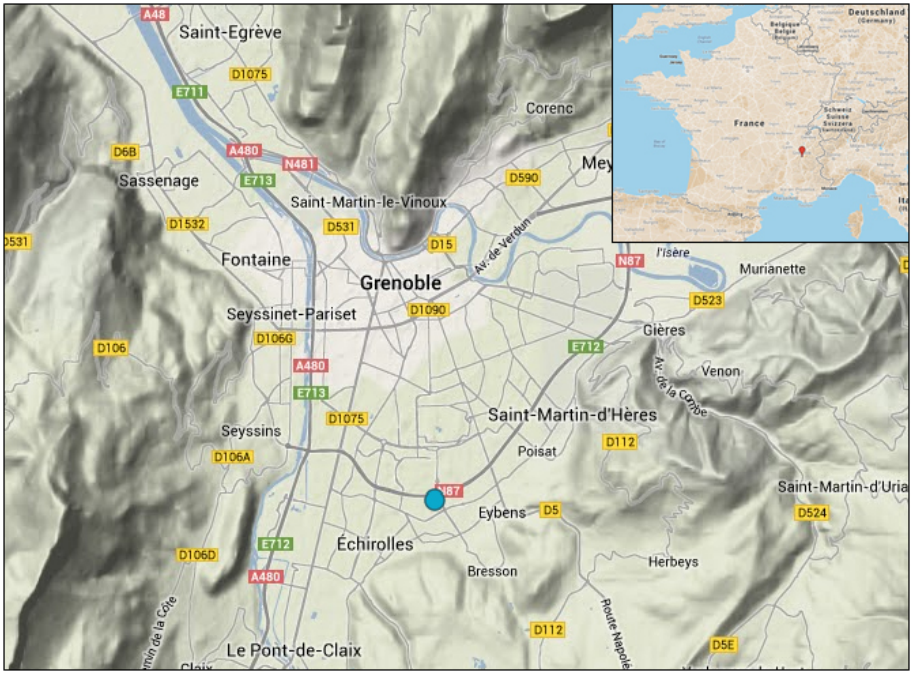

Figure 1. The measurement site is marked by a blue dot. Grenoble is to the north.

ACPD
14, 27373–27424, 2014

Direct measurements of near-highway emissions in a high diesel environment

H. L. DeWitt et al.

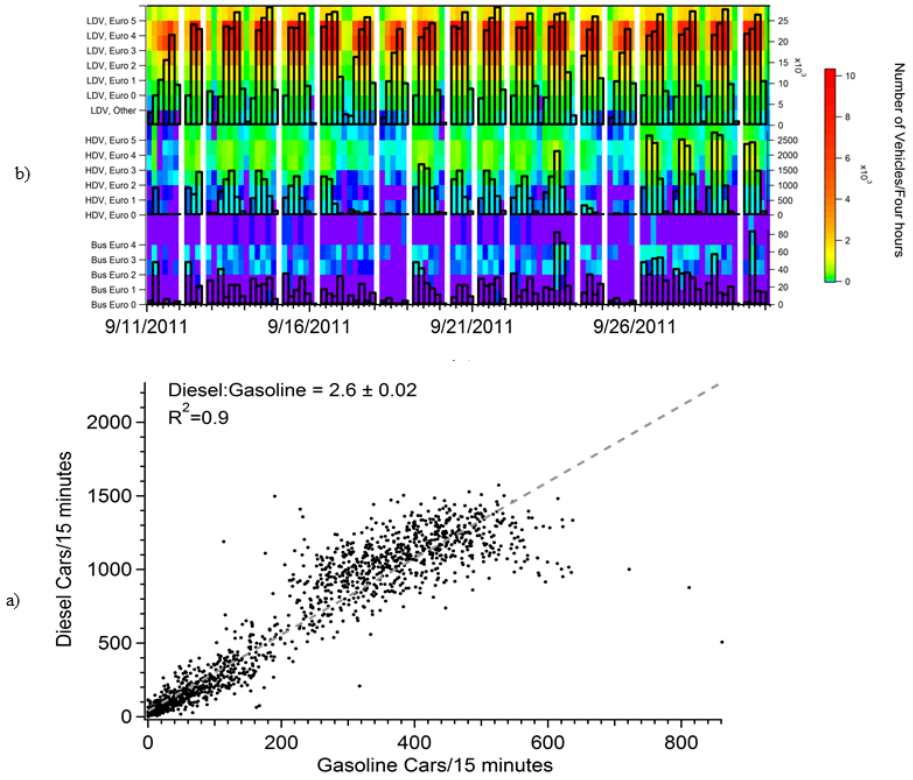

Figure 2. The number of diesel and gasoline vehicles per 15 min **(a)**. The number of bus, commercial vehicle (CV), and personal vehicle (PV) divided into Euro 0–5 categories (left axis, **b**) and the sum of Euro 0–5 for each category of vehicle (right axis, **b**). The colored squares correspond to four hour averages of vehicle concentrations (Euro 0–5).

ACPD
14, 27373–27424, 2014

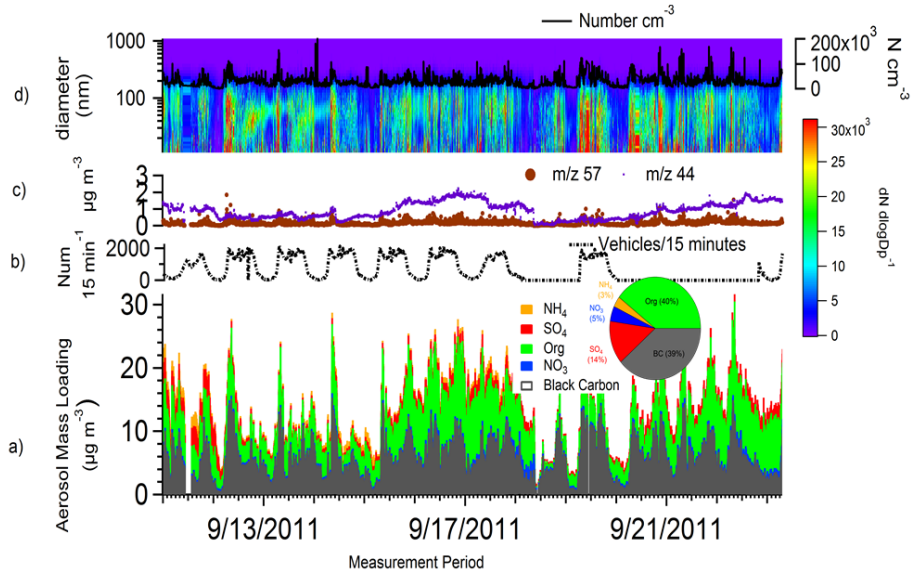

Figure 3. The non-refractory submicrometer aerosol concentration in $\mu g\,m^{-3}$ of SO_4, NH_4, NO_3, and Organic species is plotted along with black carbon **(a)**, 15 min traffic concentration (missing data due to malfunction in the traffic cameras on those days) **(b)** COO^+ (m/z 44) and $C_4H_9^+$ (m/z 57) **(c)**, and the number-weighted geometric size distribution **(d)** with the total number concentration of particles as a function of time (**d**, right axis). Inset shows the percent concentration of each species in **(a)** to the total aerosol concentration.

ACPD
14, 27373–27424, 2014

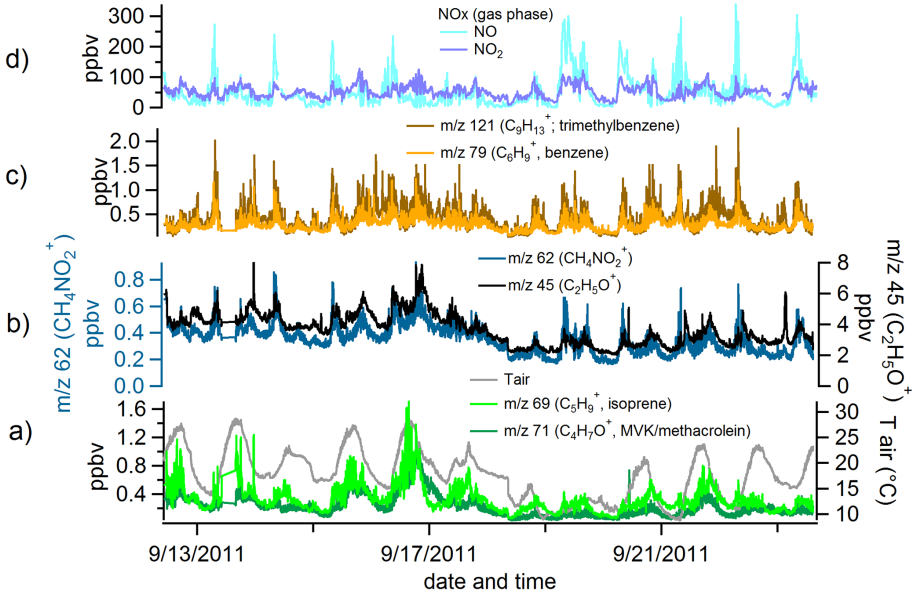

Figure 4. The concentration in ppbv of PTR-ToF-MS VOC species identified isoprene and MVK/Methacrolin (left axis, **a**), VOC species associated with diesel exhaust ($CH_4NO_2^+$, $C_2H_5O^+$), **(b)**,VOC species associated with gasoline exhaust ($C_6H_7^+$, C_9H13^+, **c**). NO and NO_2 (gas-phase) ppbv concentrations **(d)** and ambient temperature (right axis, **a**) during the measurement period are also shown.

ACPD
14, 27373–27424, 2014

Direct measurements of near-highway emissions in a high diesel environment

H. L. DeWitt et al.

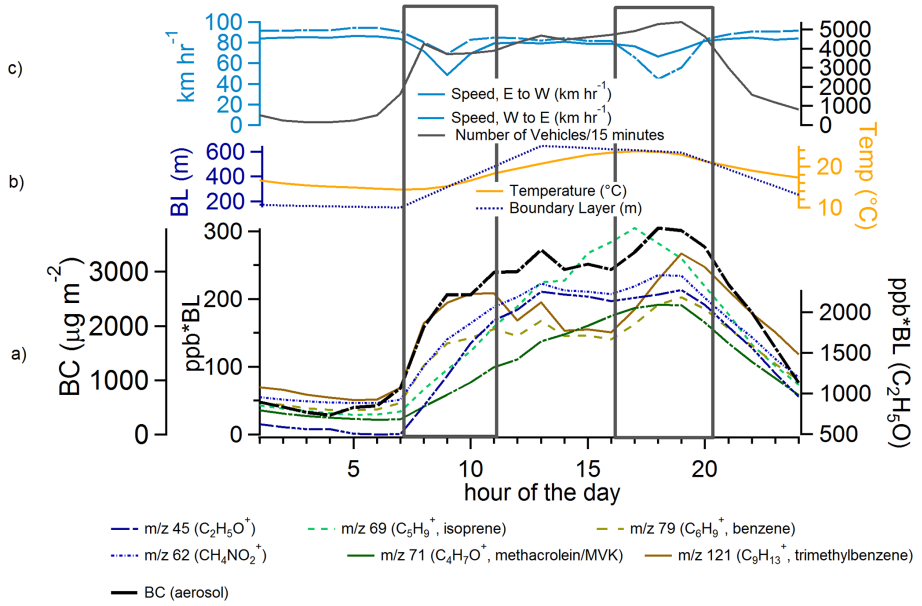

Figure 5. Diurnal profiles of boundary-layer scaled VOC peaks from PTR-MS measurements and BC peaks from MAAP measurements **(a)**, temperature (right axis, **b**), boundary layer height (left axis, **b**), vehicular speed (left axis, **c**) and vehicle concentration (right axis, **c**).

ACPD
14, 27373–27424, 2014

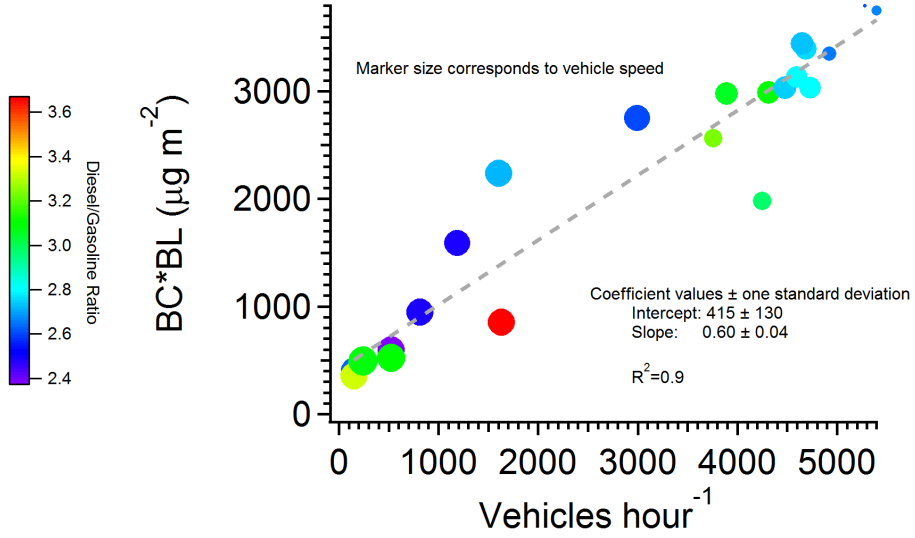

Figure 6. Diurnally averaged BC concentrations (corrected for boundary layer height) vs. diurnally averaged vehicle concentration. Colors correspond to diesel/gasoline ratio and the marker size corresponds to vehicle speed, from small (slow) to large (fast).

ACPD
14, 27373–27424, 2014

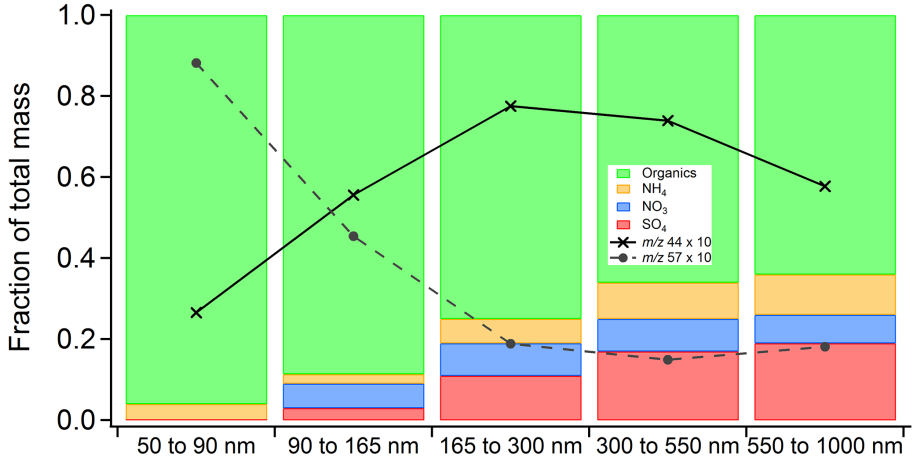

Figure 7. The SO_4, NH_4, NO_3, and organic fraction of total mass for non-refractory submicrometer aerosol particles five different size bins (**a**) and the fraction of m/z 44 and m/z 57, multiplied by 10.

ACPD
14, 27373–27424, 2014

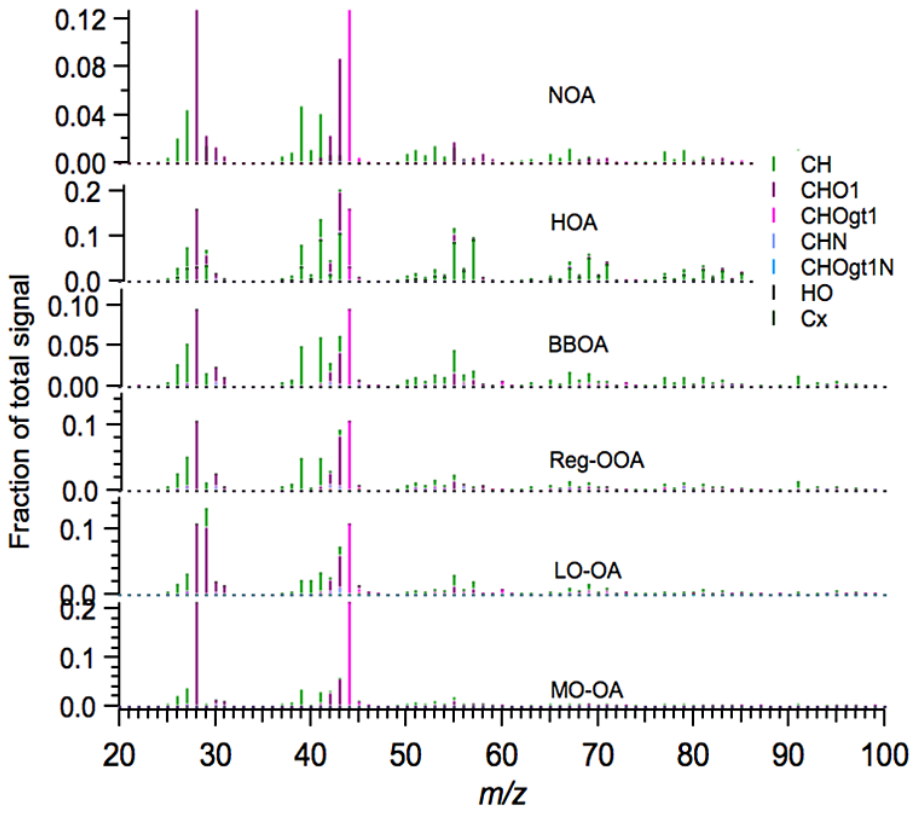

Figure 8. The mass spectra of the six resolved factors, more oxidized organic aerosol (MO-OA), less oxidized organic aerosol (LO-OA), regional oxidized organic aerosol (reg-OOA), biomass burning organic aerosol (BBOA), hydrocarbon-like organic aerosol (HOA), and nitrogen-containing organic aerosol (NOA). Fraction of total signal is plotted against m/z and the peaks are color-coded to show their high-resolution identifications.

ACPD
14, 27373–27424, 2014

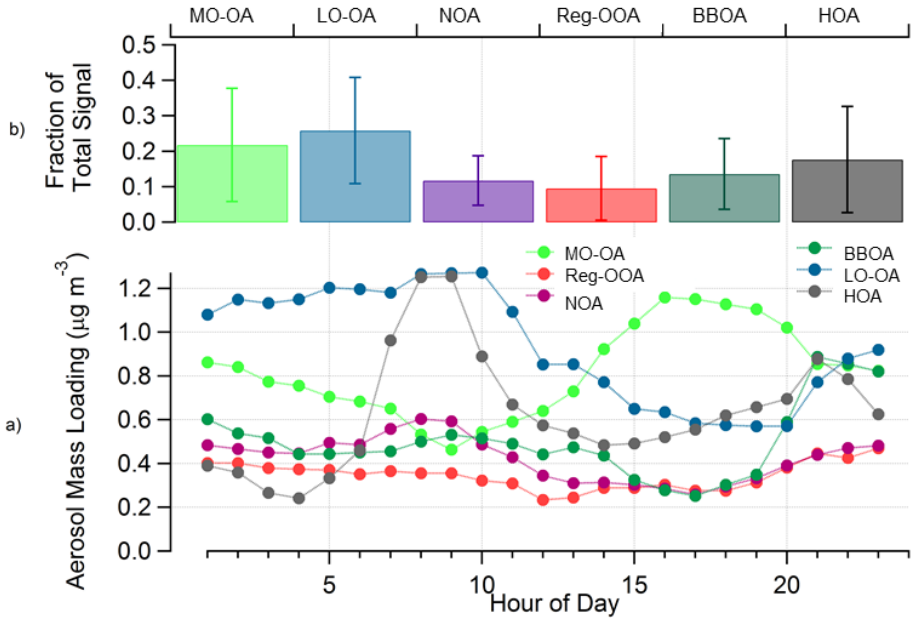

Figure 9. The diurnal profiles **(a)** and concentration and SD of the six resolved aerosol factors **(b)**.

ACPD
14, 27373–27424, 2014

Direct measurements of near-highway emissions in a high diesel environment

H. L. DeWitt et al.

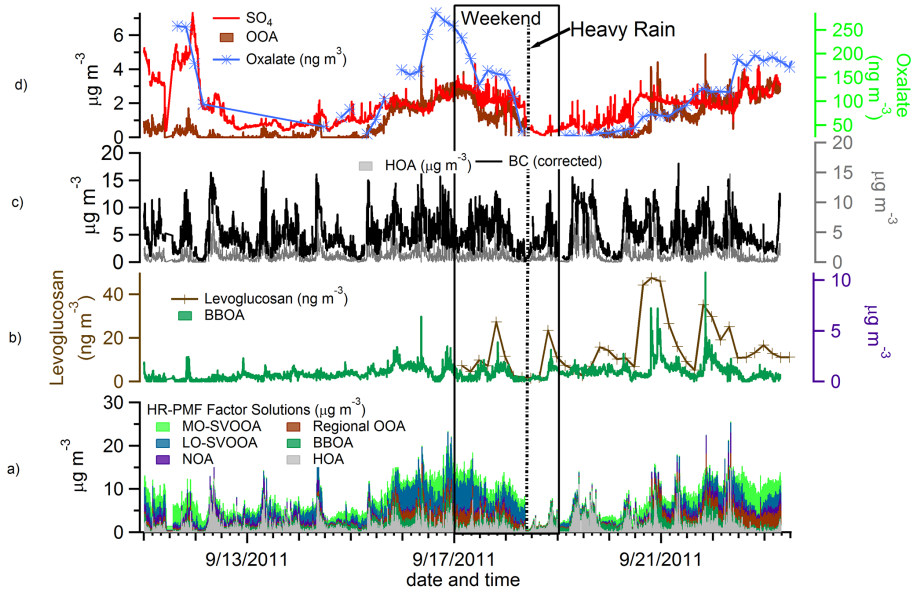

Figure 10. The time series of the six-factor PMF solution **(a)**, the resolved BBOA factor time series concentration (right axis, **b**) and off-line levoglucosan measurements (left axis, **b**), the resolved HOA factor time series concentration and BC (right axis, **c**), HR-TOF-AMS-measured SO_4 and the resolved regional OOA factor (left axis, **d**) and off-line oxalate measurements (right axis, right).

ACPD
14, 27373–27424, 2014

Direct measurements of near-highway emissions in a high diesel environment

H. L. DeWitt et al.

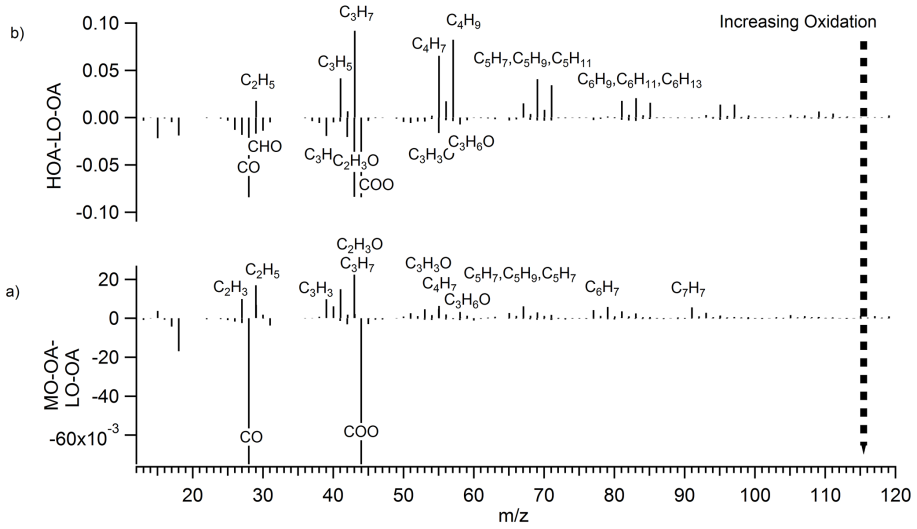

Figure 11. Difference spectra of normalized LO-OA and MO-OA **(a)** and HOA and LO-OA **(b)**.

ACPD
14, 27373–27424, 2014

Direct measurements of near-highway emissions in a high diesel environment

H. L. DeWitt et al.

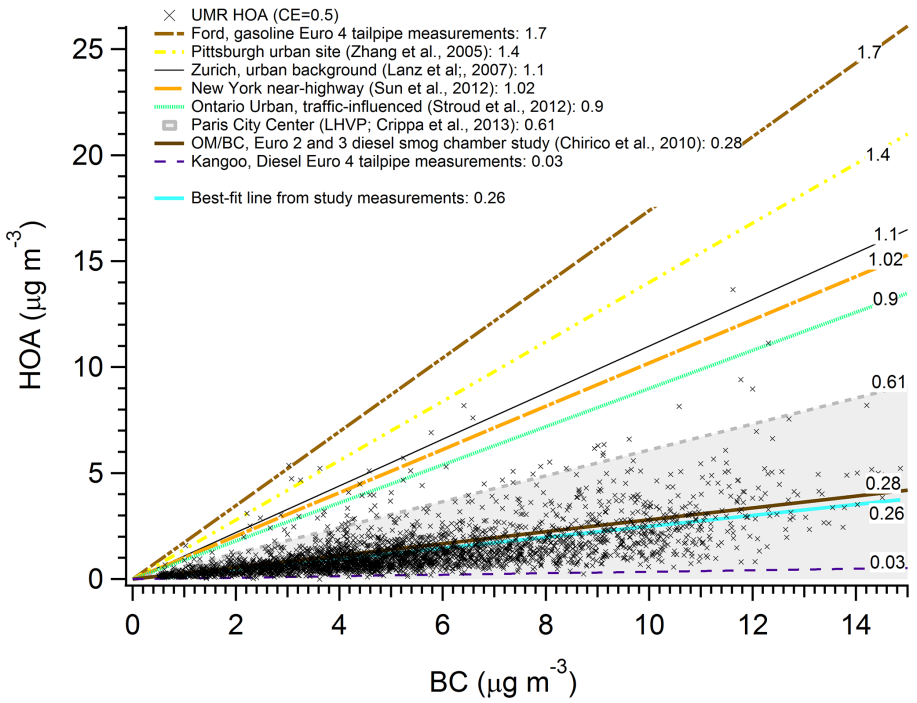

Figure 12. Calculated UMR HOA and measured BC concentrations from the campaign and HOA: BC ratios from previous field campaigns. Grey area is shaded to include a diesel-only environment and two French HOA : BC ratios: one from Crippa et al. (2013) and from this study.

ACPD
14, 27373–27424, 2014

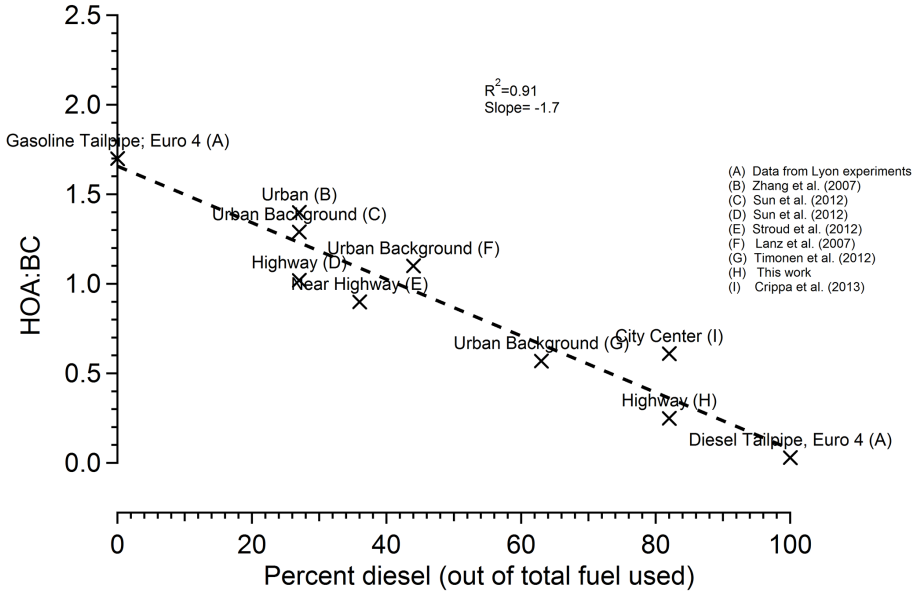

Figure 13. Comparison of the HOA : BC ratio of different field campaigns and the diesel: gasoline fuel use in each of the respective measurement locations. HOA : BC ratios and locations from Fig. 11, percent diesel fuel use from the World Bank, (2011).

ACPD
14, 27373–27424, 2014

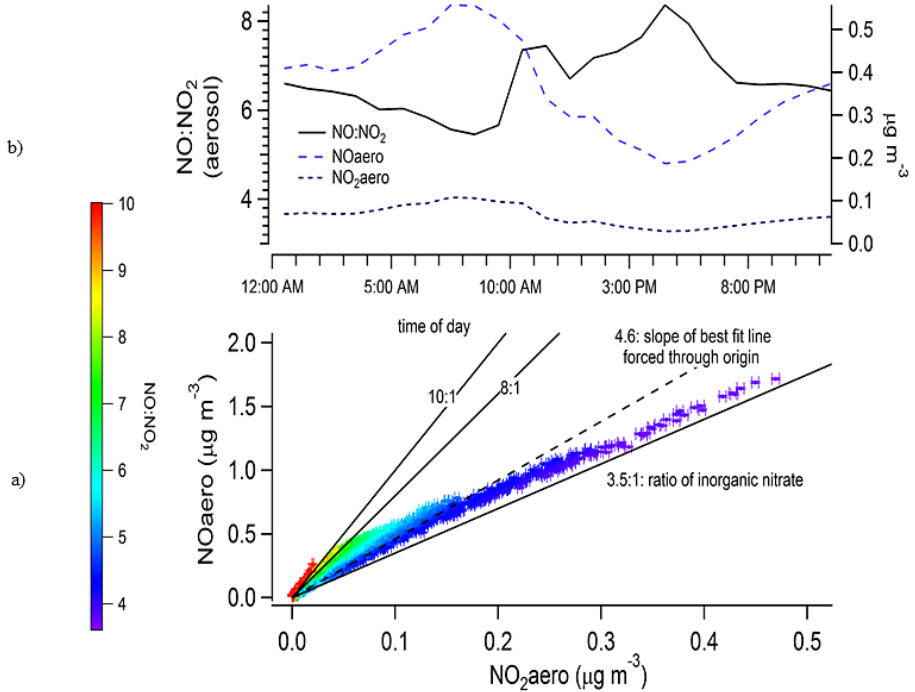

Figure 14. High resolution NO_{aero} and NO_{2aero} peaks from the HR-ToF-AMS-HR-TOF-AMS, colored by the $NO:NO_2$ ratio **(a)**. NO: NO_2 aerosol ratio diurnal profile (left axis, **b**) and NO_{aero} and NO_{2aero} HR-ToF-AMS-HR-TOF-AMS diurnal concentrations (right axis, **b**).

ACPD
14, 27373–27424, 2014

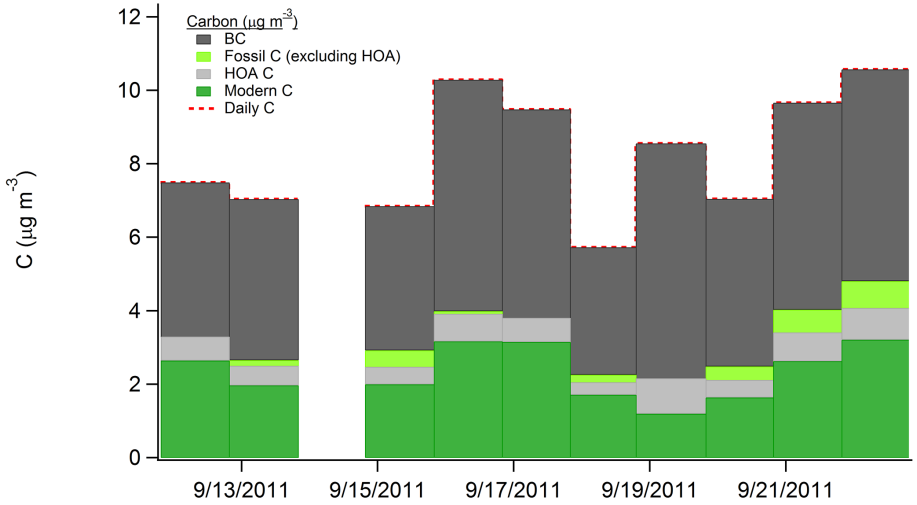

Figure 15. Daily concentration of carbon, BC, Fossil C, HOA C, and Modern C **(a)**; Total organic carbon, HOA carbon, and SOA carbon vs. fossil organic carbon **(b)**.

ACPD
14, 27373–27424, 2014